From the Department of Clinical Sciences and Education,
Södersjukhuset,
Karolinska Institutet, Stockholm, Sweden

Echocardiography in Myocardial Infarction — Aspects on Diastolic Function and Evaluation by Cardiovascular Magnetic Resonance Imaging

Martin G. Sundqvist, M.D.

Karolinska Institutet

Stockholm 2023

Published by Karolinska Institutet.
Printed by Universitetsservice US-AB, 2023.

ISBN 978-91-8016-866-3
An electronic version of this thesis can be found online at openarchive.ki.se.
Cover illustration: Damped harmonic motion.

Echocardiography in Myocardial Infarction — Aspects on Diastolic Function and Evaluation by Cardiovascular Magnetic Resonance Imaging

Thesis for Doctoral Degree (Ph.D.)

By

Martin G. Sundqvist

The thesis will be defended in public at the Aula, Södersjukhuset, Stockholm, February 10th, 2023.

Principal Supervisor:
Professor Martin Ugander, M.D., Ph.D.
Karolinska Institutet
Department of Molecular Medicine and Surgery

Co-supervisor:
Professor Per Tornvall, M.D., Ph.D.
Karolinska Institutet
Department of Clinical Science and Education, Södersjukhuset

Opponent:
Professor Sherif F. Nagueh, M.D.
Houston Methodist Weill Cornell Medical College
Departments of Cardiology and Cardiovascular Sciences

Examination Board:
Professor Frank Flachskampf, M.D., Ph.D.
Uppsala University
Department of Medical Sciences

Associate Professor Ellen Ostenfeld, M.D., Ph.D.
Lund University
Department of Clinical Sciences

Professor Odd Bech-Hanssen, M.D., Ph.D.
Gothenburg University
Department of Molecular and Clinical Medicine

Ut tensio, sic vis
— *Robert Hooke*, 1678

Popular science summary of the thesis

The function of the heart can be studied using different technologies that produce images and short film clips, as well as graphical depictions of measurements such as blood flow velocities over time, etc. The most common imaging modality is echocardiography, which involves using ultrasound to study the heart. Many echocardiographic methods have been used to study diastolic function, which refers to the filling of the heart with blood between heart beats. In this thesis a software application for studying aspects of diastolic function using a mathematical model was produced and made publicly available (www.echoewaves.org, Study I), and normal values for the model were proposed after analyzing a cohort of patients with otherwise normal examinations (Study II).

In Study III cardiovascular magnetic resonance imaging (CMR) was used to measure the amount of dead and/or swollen tissue after a heart attack, and the relationship between those amounts and various parameters used to study diastolic function was analyzed. It was found that the amount of dead and swollen tissue, respectively, did not seem to have a clear effect on diastolic function.

In Study IV echocardiography and CMR was used to study patients with clinically suspected heart attacks, where the work-up had ruled out obstruction of a coronary artery. Coronary obstruction is a prerequisite for a typical heart attack, and the studied patient group was found to have a mix of different diagnoses using CMR. The focus of the study was to examine if echocardiography, which is much more readily available than CMR, could be used to select patients for CMR. It was found that even in patients with normal echocardiograms, many patients still receive a diagnosis by CMR imaging, implying that CMR should be routinely used in this clinical setting.

Abstract

Background

Echocardiography is routinely used to evaluate patients with known or suspected myocardial infarction (MI). Cardiovascular magnetic resonance imaging (CMR) provides the ability to quantify myocardial infarction size (IS), and to establish an underlying diagnosis in MI cases with nonobstructive coronary arteries (MINOCA). While echocardiography provides valuable information regarding cardiac function, the relationships between how pathology is manifested on CMR, and the information gleaned from echocardiography are not fully explored. The focus of this thesis was 1) to assess diastolic function and mechanics in MI, and 2) to assess the ability of echocardiography to identify patients needing further evaluation by CMR in MINOCA.

Methods and results

In **Study I,** a software application was developed for the purpose of facilitating the analysis of diastolic function using the parameterized diastolic filling (PDF) method. Inter- and intraobserver variability was studied using patients from Study III and Study IV. The software was successfully developed and made publicly available at www.echoewaves.org, and inter- and intraobserver reliability was good or excellent for most PDF measures (intraclass correlation coefficient 0.80-0.99).

In **Study II**, an available clinical database of patients undergoing resting and stress echocardiography was used to identify a cohort of patients with normal echocardiographic findings. PDF analysis was performed in 138 patients for the establishment of normal reference values for the method, and presented as sex-specific 95% reference intervals.

In **Study III**, a pre-planned substudy of the RECOND trial, the association between myocardial infarction size (IS) and parameters of diastolic function, and whether the peri-infarction edema of the myocardium at risk (MaR) influenced these relationships was investigated. Weak associations were found between IS and deceleration time ($R^2 = 0.24$, $p < 0.001$), left atrial volume index ($R^2 = 0.13$, $p = 0.01$), and the PDF stiffness parameter k ($R^2 = 0.21$, $p < 0.001$). The only parameter influenced by the addition of MaR was e′ (increase in adjusted $R^2 = 0.08$, $p = 0.02$). The PDF damping parameter c was the only parameter associated with final IS at 6 months follow-up ($R^2 = 0.22$, $p = 0.001$).

In **Study IV,** a pre-planned substudy of the SMINC2 study, the value of normal vs pathological echocardiography, as well as the blood biomarkers hs-TnT and NT-pro-BNP, for selecting patients presenting with MINOCA for further evaluation with CMR was investigated. Pathological echocardiography identified patients with a CMR diagnosis with sensitivity 77%, specificity 38%, positive predictive value 82%, and negative

predictive value 30%. At low levels of hs-TnT and NT-pro-BNP, the probability of obtaining a diagnosis by CMR was still substantial (> 25%).

Conclusions and summary

In summary, a freely available and reliable software application for the application of the PDF method was developed (Study I), and normal reference limits were provided, for use in further clinical research (Study II). IS as measured by CMR does not seem to be a major determinant of diastolic dysfunction after MI, and other factors are likely to be more important (Study III). CMR is a valuable diagnostic tool for the evaluation of patients with MINOCA, even when echocardiographic examinations are normal, and levels of hs-TnT and NT-pro-BNP are low (Study IV).

List of scientific papers

I. **Sundqvist MG**, Salman K, Tornvall P, Ugander M.

Kinematic analysis of diastolic function using the freely available software Echo E-waves - feasibility and reproducibility.
BMC Medical Imaging 2016;16:60.

II. **Sundqvist MG**, Sahlén A, Ding ZP, Ugander M.

Normal reference values for assessing diastolic function using the parameterized diastolic filling formalism method in patients with normal results of rest and stress echocardiography.
Ultrasound in Medicine & Biology 2018;44(11):2261-2266.

III. **Sundqvist MG**, Verouhis D, Sörensson P, Henareh L, Persson J, Saleh N, Settergren M, Witt N, Böhm F, Pernow J, Tornvall P, Ugander M.

The size of myocardial infarction and peri-infarction edema are not major determinants of diastolic impairment after acute myocardial infarction.
Submitted. Preprint doi.org/10.1101/2022.07.01.22277049.

IV. **Sundqvist MG**, Sörensson P, Ekenbäck C, Lundin M, Agewall S, Bacsovics Brolin E, Cederlund K, Collste O, Daniel M, Jensen J, Y-Hassan S, Henareh L, Hofman-Bang C, Lyngå P, Maret E, Sarkar N, Spaak J, Winnberg O, Caidahl K, Ugander M, Tornvall P.

Cardiovascular magnetic resonance imaging commonly identifies a definitive diagnosis following normal echocardiography in myocardial infarction with nonobstructed coronary arteries.
Submitted. Preprint doi.org/10.1101/2022.10.25.22281518.

Scientific papers not included in the thesis

I. Collste O, Alam M, **Sundqvist M**, Olson J, Wardell J, Tornvall P, Frick M. Vulnerability to sympathetic stress does not persist in takotsubo stress cardiomyopathy. *Journal of Cardiac Failure* 2014;20(12):968-72.

II. Verouhis D, Sörensson P, Gourine A, Henareh L, Persson J, Saleh N, Settergren M, **Sundqvist M**, Tornvall P, Witt N, Böhm F, Pernow J. Effect of remote ischemic conditioning on infarct size in patients with anterior ST-elevation myocardial infarction. *American Heart Journal* 2016;181:66-73.

III. Tornvall P, Brolin Eb, Caidahl K, Cederlund K, Collste O, Daniel M, Ekenbäck C, Jensen J, Y-hassan S, Henareh L, Hofman-bang C, Lyngå P, Maret E, Sarkar N, Spaak J, **Sundqvist M**, Sörensson P, Ugander M, Agewall S. The value of a new cardiac magnetic resonance imaging protocol in Myocardial Infarction with Non-obstructive Coronary Arteries (MINOCA) - a case-control study using historical controls from a previous study with similar inclusion criteria. *BMC Cardiovascular Disorders* 2017;17(1):199.

IV. Salman K, Cain PA, Fitzgerald BT, **Sundqvist MG**, Ugander M. Cardiac Amyloidosis Shows Decreased Diastolic Function as Assessed by Echocardiographic Parameterized Diastolic Filling. *Ultrasound in Medicine & Biology* 2017;43(7):1331-1338.

V. Hendrikx T, **Sundqvist M**, Sandström H, Sahlin C, Rohani M, Al-Khalili F, Hörnsten R, Blomberg A, Wester P, Rosenqvist M, Franklin K. Atrial fibrillation among patients under investigation for suspected obstructive sleep apnea. *PloS One* 2017;12(2):e0171575.

VI. Ljung L, **Sundqvist M**, Jernberg T, Eggers KM, Ljunggren G, Frick M. The value of predischarge exercise ECG testing in chest pain patients in the era of high-sensitivity troponins. *European Heart Journal. Acute Cardiovascular Care* 2018;7(3):278-284.

VII. Elfwén L, Hildebrand K, Schierbeck S, **Sundqvist M**, Ringh M, Claesson A, Olsson J, Nordberg P. Focused cardiac ultrasound after return of spontaneous circulation in cardiac-arrest patients. *Resuscitation* 2019;142():16-22.

VIII. Goldberg YH, Megyessi D, Flam M, Spevack DM, **Sundqvist MG**, Ugander M. Mechanistic validation of the 2016 American Society of Echocardiography/European Association of Cardiovascular Imaging Guidelines for the assessment of diastolic dysfunction in heart failure with reduced ejection fraction. *Cardiovascular Ultrasound* 2020;18(1):42.

IX. **Sundqvist MG**, Sahlén A, Ding ZP, Ugander M. Diastolic function and its association with diabetes, hypertension and age in an outpatient population with normal stress echocardiography findings. *Cardiovascular Ultrasound* 2020;18(1):46.

X. Verouhis D, Sörensson P, Gourine A, Henareh L, Persson J, Saleh N, Settergren M, **Sundqvist M**, Tengbom J, Tornvall P, Witt N, Böhm F, Pernow J. Long-term effect of remote ischemic conditioning on infarct size and clinical outcomes in patients with anterior ST-elevation myocardial infarction. *Catheterization and Cardiovascular Interventions* 2021;97(3):386-392.

Contents

List of abbreviations

ACS	Acute coronary syndrome
AT	Acceleration time
CI	Confidence interval
CMR	Cardiovascular magnetic resonance imaging
DICOM	Digital imaging and communications in medicine
DT	Deceleration time
DVP	Doppler velocity profile
GLS	Global longitudinal strain
hs-TnT	High sensitive troponin T
ICC	Intraclass correlation
IQR	Interquartile range
IS	Myocardial infarction size
KFEI	Kinematic filling efficiency index
LAP	Left atrial pressure
LGE	Late gadolinium enhancement
LV	Left ventricle/left ventricular
LVEF	Left ventricular ejection fraction
MaR	Myocardium at risk
MI	Myocardial infarction
MINOCA	Myocardial infarction with nonobstructive coronary arteries
NSTEMI	Non-ST-elevation myocardial infarction
PCI	Percutaneous coronary intervention
PDF	Parameterized diastolic filling
PW	Pulsed wave
RECOND	Reduction in Infarct Size by Remote Per-postconditioning in Patients With ST-Elevation Myocardial Infarction
RWMA	Regional wall-motion abnormality
SMINC2	Stockholm myocardial infarction with normal coronaries 2
SPECT	Single-photon emission computed tomography
STEMI	ST-elevation myocardial infarction
TDI	Tissue Doppler imaging
TTS	Takotsubo syndrome
Vmax	Maximum velocity
VTI	Velocity time integral

1 Introduction

Echocardiography is the most frequently employed imaging modality in contemporary cardiology. It can provide a wide array of measurements claiming to reflect not only various aspects of cardiac function, but also patterns of findings indicating underlying diagnoses and prognosis. Despite its ubiquitous application in such a commonly occurring condition as myocardial infarction (MI), many aspects of the interpretation of echocardiography remain to be more fully elucidated. In this thesis, some ways of using echocardiography are explored, and compared to findings from cardiovascular magnetic resonance imaging, a method which in many cases can provide useful insights regarding the presence and extent of MI and other disease processes. Specifically, the thesis focuses on diastolic function, which is how the heart fills with blood, and how MI can affect it, and secondly how echocardiography can be used in the group of patients with MI without obstruction of the coronary arteries, using cardiovascular magnetic resonance imaging as a reference.

2 Literature review

2.1 Cardiac structure and function as assessed by imaging

The heart is a complex organ and an exhaustive description of its anatomy, biology, and physiology is beyond the scope of this thesis. This thesis will address background relevant to the herein presented studies. The heart has four chambers, of which the left ventricle (LV) and left atrium (LA) are of particular for the study of MI and diastolic function. The LA receives oxygenated blood from the lungs and the LV takes this blood and ejects it into the aorta, from which it is further distributed to the rest of the body. The ventricles are primarily composed of muscle cells, cardiomyocytes, of which the sarcomere is the smallest subcellular functional unit. The sarcomere contains the contractile apparatus with actin, myosin, and the troponin complex. While these molecular structures can generate force and shorten the sarcomeres and the myocardium they are joined in, they do not restore the length of the sarcomere between contractions. Instead, the giant Titan protein, or titin for short, bestows elastic properties to cardiac muscle, acting much like a biological spring. While contraction consumes energy, some of the kinetic energy is stored as potential energy in the compressed titin structures, subsequently to be used to recoil titin, and the sarcomeres, to their resting state. During this recoil there is energy expenditure to release the tension caused by contraction, but not to restore the length of the contractile unit, the latter being caused by passive tissue properties.

While these mechanisms at the subcellular, cellular, and tissue levels are well documented, they are not directly available for examination using the two most commonly employed modalities for imaging of cardiac function *in vivo*, namely echocardiography and cardiovascular magnetic resonance imaging (CMR).

2.1.1 Echocardiography

An echocardiography scanner transmits ultrasound waves into the examined patient's body, and the reflected signal can be constructed as still or moving images. This is possible since different tissues reflect different amounts of ultrasound. Furthermore, the velocity of blood or tissues can be measured by utilizing the Doppler shift that occurs when the transmitted wave is reflected by a moving reflector. Still images are used mainly for measuring the size of different structures, such as LV volume. Moving images are used to assess function, where the above-described contraction-recoil pattern can be seen as radial wall thickening secondary to the longitudinal contraction that causes the LV to shorten from base to apex, with recoil rapidly restoring LV length accompanied by radial wall thinning. Wall thickening is normally synchronous and homogeneous, and deviations are described as regional wall motion abnormalities (RWMA). Global systolic function is most often parameterized as the ratio between

ejected blood (stroke volume) and end-diastolic volume, termed left ventricular ejection fraction (LVEF), or as the average longitudinal shortening of the LV, termed global longitudinal strain (GLS).

For the purposes of this thesis, special emphasis is put on pulsed wave (PW) Doppler. In a PW Doppler examination, short bursts of ultrasound waves are emitted in a narrow beam, and the scanner then waits for a period before sampling the returning signal. The waiting time is determined by the depth from which the velocities are to be interrogated, and the time is calculated assuming constant velocity of ultrasound propagation through the body. By changing beam angle and depth, a sample volume can be placed at, for example, the mitral valve opening for measuring the blood flow velocities during LV filling. PW Doppler has a temporal resolution of > 500 samples per second that can be stored in the final image, but it is limited by only being able to accurately measure blood flow that is parallel to the ultrasound beam. The velocities of blood flow are approximately ten times higher than the velocities of cardiac muscle motion, but the amplitude of the blood flow signal is much lower. By filtering high velocities and not amplifying low amplitude signals, the velocities of tissue moving through the sample volume can be measured. This is called tissue Doppler imaging (TDI). PW Doppler and TDI are essential for the study of diastolic function[1,2] as discussed in further detail below in Section 2.3.

2.1.2 Cardiovascular magnetic resonance imaging

When placed in a strong magnetic field, differences in tissue composition will lead to differences in response to radiofrequency (RF) excitation of the tissues. This is exploited by CMR to visualize anatomy and function in a similar fashion to what is done in echocardiography. However, CMR can also provide information on tissue characteristics by providing quantitative or semi-quantitative information on differences in fat and water content in an image. This can be used to visualize myocardial edema, since edematous parts of a tissue will have increased water content. CMR is routinely performed with administration of a gadolinium-based contrast agent. These contrast agents have an extracellular distribution that is increased in areas with damaged cell membranes or expanded extracellular space such as after cell destruction. This makes it possible to visualize scarring after disease processes such as myocarditis and MI by imaging using a technique called late gadolinium enhancement (LGE). LGE has very good agreement with the extent of myocardial infarction[3], making it possible to quantify the volume of infarcted myocardium. This makes it possible to study how myocardial infarction size (IS) affects cardiac function and prognosis. It has been established that larger IS is associated with worse prognosis both using CMR[4], and earlier with single-photon emission computed tomography (SPECT)[5,6].

Different LGE patterns have also been associated with different diseases[7], notably differentiating ischemic lesions, characterized by mostly endocardial distributions compatible with coronary perfusion territories, from non-ischemic lesions characterized by mid-wall, epicardial or patchy distributions. Using these LGE patterns in conjunction with other findings, including distribution of edema and regional and global assessment of function, it is possible to confidently propose a diagnosis of *e.g.*, myocardial infarction, myocarditis, or amyloidosis. Compared to echocardiography, which can only produce images where the ultrasound beam can be transmitted and reflected back to the probe, CMR is not limited by anatomical constraints. However, echocardiography typically has a much higher temporal resolution, especially using Doppler-based methods. While assessment of diastolic function is possible using CMR[8,9], it is not yet widely used clinically for this purpose.

2.2 Myocardial injury and infarction

As described above, troponins are regulatory proteins in the contractile apparatus of the myocardium. Most pathological processes affecting the heart, but also physiological stress such as intense exercise, can lead to a release of troponin into the blood stream, where its concentration can be analyzed using modern high-sensitivity methods (high-sensitive troponin T [hs-TnT]). Any condition causing an elevation above the 99th percentile of the analysis method's upper reference limit has by definition caused myocardial injury, while myocardial infarction is defined as cellular necrosis caused by ischemia which invariably also will cause an elevation of hs-TnT. Myocardial infarction can then be classified further according to its etiology, with types 1 and 2 being of interest for this thesis. Both are characterized by a rise or fall in hs-TnT accompanied by ischemic symptoms, new ECG changes, and/or findings of new RWMA or evidence of loss of viable myocardium[10]. The difference between type 1 and 2 MI is that type 1 is caused by atherothrombotic coronary artery disease, while type 2 is caused by a mismatch in oxygen supply and demand to the myocardium. When assessed by cardiac imaging, MI manifests itself as RWMA and sometimes global dysfunction, and additionally as LGE with an ischemic pattern by CMR.

2.2.1 The myocardium at risk

In type 1 MI caused by coronary obstruction, a larger portion of the myocardium can initially suffer from ischemia than that which will finally undergo necrosis. The larger area is referred to as the myocardium at risk for infarction (MaR). The degree of coronary obstruction can vary, due to autolysis of thrombi, which can alleviate the extent and duration of ischemia. Restoration of blood flow and minimization of final IS is also the goal of standard care for patients with suspected acute coronary occlusion[11].

When the studies included in this thesis were performed it was generally considered that the edema surrounding the MI represented the MaR. However, there has been

controversy about what the visualized edema represented pathophysiologically[12,13], and according to a recent expert panel the extent of the edema is affected both by the size of the MaR, but also the characteristics of reperfusion injury as potentially modified by various treatments[14]. This has consequences for studying the concept of myocardial salvage (the difference between potential [MaR] and actual IS), but not necessarily for studying what effect edema *per se* has on myocardial function.

2.2.2 Myocardial edema as a cause of functional impairment

It has been shown that myocardial edema of various causes can affect myocardial function even in the absence of infarction[15], and that experimentally induced edema can impair both systolic and diastolic function[16–19]. How these latter experimental studies translate to naturally occurring myocardial edema in the setting of disease is not clear. It has also been shown that regional systolic function is decreased in the MaR[20].

2.2.3 The concept of a working diagnosis in acute coronary syndromes

Finding the underlying diagnosis of myocardial injury may require several diagnostic tests and observation over time. However, as myocardial infarction needs urgent management, it is to be approached as a working diagnosis based on history, ECG, and laboratory findings. This has led to the recognition of acute coronary syndrome (ACS) with or without ST-elevation on the ECG (STE-ACS/NSTE-ACS) to be recognized as working diagnoses, used to trigger urgent treatment, valid until further investigations either confirm MI as the final diagnosis (STEMI/NSTEMI) or indicate other pathology.

2.2.4 MINOCA as a working and final diagnosis

In many studies 5-9% of patients presenting with symptoms leading to a working diagnosis of an ACS and fulfilling clinical criteria for MI, do not have coronary artery disease of sufficient severity to be likely to cause MI[21–23]. These patients are said to have a working diagnosis of myocardial infarction with nonobstructive coronary arteries (MINOCA)[10,24]. This working diagnosis warrants further investigation, as many of these patients will turn out to have non-ischemic disease with presentation suggestive of ACS, but not caused by MI. Having ruled out other causes, and if possible having found evidence of MI using CMR, a final diagnosis of MINOCA can be made. Thus, MINOCA can be both a temporary working diagnosis and a final diagnosis. In patients with MINOCA as a working diagnosis, common final diagnoses are MI (which can be due to plaque rupture, spasm, dissection, or thromboembolism, *etc.*), myocarditis, and takotsubo syndrome, or other non-cardiac etiologies such as pulmonary embolism[22,25–27]. The work-up of MINOCA as a working diagnosis can span the spectrum of cardiac investigations including coronary imaging with intravascular ultrasound and optical coherence tomography, echocardiography, CMR, nuclear imaging, cardiac computed tomography angiography, ECG monitoring, coronary spasm provocation, and blood tests.

2.3 Diastolic function

The cardiac cycle is conventionally divided into two time periods, systole and diastole, defined by the opening and closing of the valves. Blood is ejected from the ventricles during systole and refilled during diastole. During early diastole the pressure in the LV is dropping, and when it falls below that of the LA, blood is sucked into the LV. This is called the early filling period. This is followed by diastasis, a time period typically with little or no transmitral flow, whereafter atrial contraction leads to more blood entering into the LV, constituting the late filling period. As mentioned above (2.1), at the subcellular level, ventricular sarcomere shortening is followed by relaxation which leads to tension release, and passive recoil restoring the length of the sarcomere.

2.3.1 Invasive evaluation of diastolic function

Relaxation due to cross-bridge detachment in the contractile apparatus cannot be measured directly, at least using clinically available methods. However, the pressure decay that it leads to can be measured invasively with a pressure catheter in the LV. The pressure decay over time can be fit to an exponential function with the time constant tau (τ), measured in milliseconds, used to assess the relaxation part of diastolic function[28]. This was initially formulated as $P(t) = P_0 e^{-t/\tau}$. If relaxation is efficient, pressure will drop rapidly, and tau will be short. Conversely, impaired relaxation will prolong tau.

By definition, the tendency of an elastic physical body to return to its original shape after deformation, *i.e.*, its tendency to recoil, is described by its stiffness. Stiffness can generally be expressed as $^{\Delta stress}/_{\Delta strain}$ which in the LV can be specified as $^{\Delta P}/_{\Delta V}$, the slope of the pressure-volume relationship. As with tau, stiffness can be measured invasively.

The pressures at which filling occur are of special interest. Both relaxation, expressed as tau, and stiffness have an association with LV pressure. Tau describes the time course of change in pressure during isovolumetric relaxation, and stiffness describes the relationship between volume and pressure. It also follows that an increase in stiffness leads to a need for higher filling pressures. In order to move blood from the LA to the LV, the pressure in the LA must be higher than in the LV, and as there are no valves between the LA and the pulmonary circulation, increased filling pressures will lead to higher mean pressures in the pulmonary circulation, a foundational component of LV backward failure.

As diastolic function depends on the interplay between relaxation, stiffness, and filling pressure, it is evident that simple parameters are unlikely to be able to describe it in an accurate or meaningful way. By contrast, systolic function is usually reduced to simple deformation imaging parameters such as LVEF or GLS, using data from only two time

points during systole, discarding all time-resolved information. While this approach has been used for inclusion criteria in successful heart failure drug trials, these parameters do not describe systolic function in any nuanced way, and there are no clear non-invasive imaging counterparts when it comes to quantitative assessment of diastolic function. That said, measures such as LV end-diastolic pressure or pulmonary artery wedge pressure provide non-imaging-based invasive alternatives.

2.3.2 Conventional echocardiographic evaluation of diastolic function

The invasive assessment of diastolic function described above can be sophisticated but is not practical as a method for routine investigation, and it is certainly not non-invasive. In 1982 Kitabatake proposed PW Doppler interrogation of transmitral flow as a method for studying diastolic function non-invasively[29]. PW Doppler records blood flow velocities, and these velocities are driven by instantaneous pressure differences. Consequently, the PW Doppler recording contains time-resolved data on pressure differences between the LA and LV, and using this information one can attempt to infer various properties of the chambers. Using PW Doppler, early filling is represented by the early (E) wave, and late filling by the atrial (A) wave. The E- and A-waves are illustrated in Figure 1. Key points of evaluation are the relationship between the E- and A-wave velocities (E/A-ratio), the acceleration and deceleration times of the E-wave (AT and DT, respectively), and the maximum velocity (Vmax) of the E-wave. Several studies have drawn direct parallels to invasive studies, *e.g.*, demonstrating that increased LV stiffness shortens the DT[30]. That said, PW Doppler examination of diastole has come to be focused on flow patterns, mainly integrating combinations of the E/A ratio and E-wave DT. These patterns were initially observed in heterogenous patient groups[31,32] rather than on a continuum of decreasing diastolic function caused by the same underlying disease.

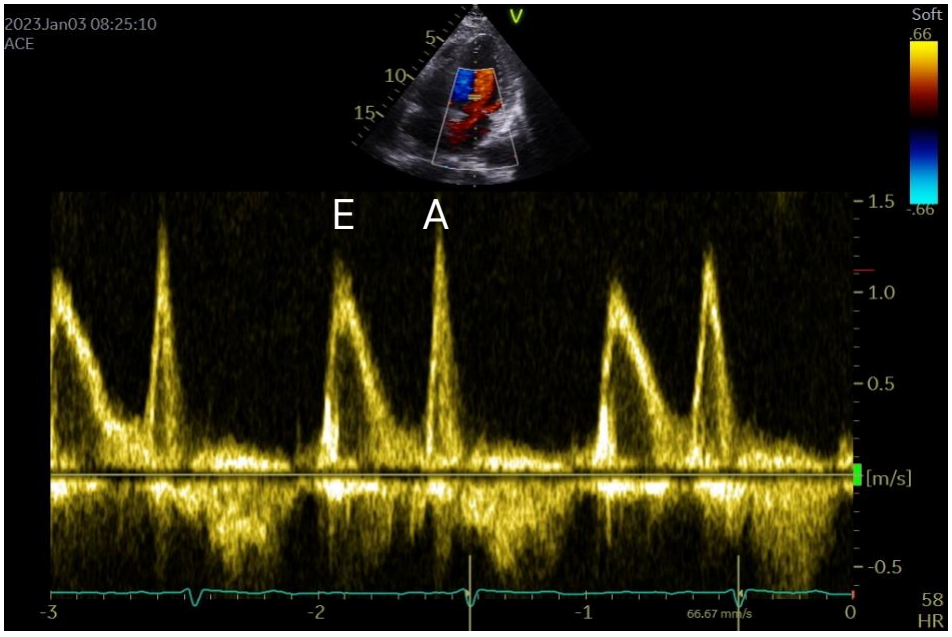

Figure 1. Mitral inflow as visualized by PW-Doppler. X-axis displays time (s), y-axis velocity (m/s). Three cardiac cycles are shown, with the E- and A-waves marked in the middle one.

There is a large body of studies of TDI investigations into diastolic function, but the parameter that has gained the most interest is the mitral annular velocity during early diastole, e'. This is the longitudinal component of LV lengthening velocity, and it has an obvious association with LV recoil. This parameter is also of special value as e' increases when LA pressure increases in hearts with normal relaxation, but remains unchanged when relaxation is impaired[33,34]. A representative example of TDI is presented in Figure 2. As the Vmax of the E-wave (E) is driven by the pressure difference between the LA and the LV, E will increase while e' remains unchanged as LA-pressure increases in left ventricles with abnormal relaxation. Because of this, the ratio of E/e' can be used to assess LA filling pressures[35,36].

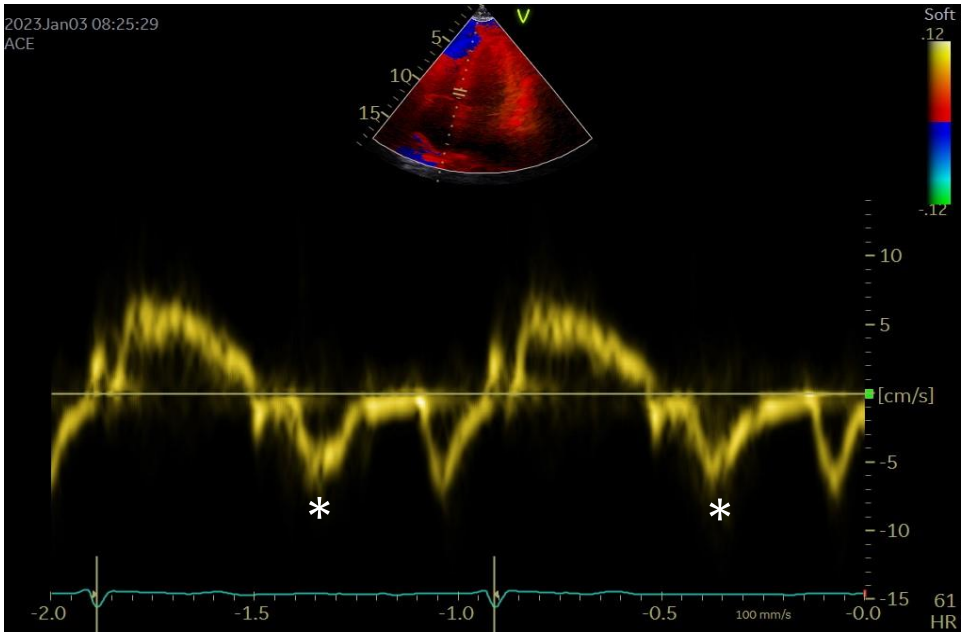

Figure 2. TDI recording of myocardial velocities. X-axis displays time (s), y-axis velocity (cm/s). The e'-waves of two consecutive cardiac cycles are marked with asterisks.

The current recommendations for assessment of diastolic dysfunction use the mitral inflow patterns, E/e', and indirect indicators of raised LA pressure in the form of LA volume and pulmonary hypertension to grade diastolic dysfunction, focusing on identifying patients with increased LA pressure[1,2]. While this grading algorithm has good interobserver variability for identifying raised filling pressures[37], many patients will also have indeterminate diastolic function[38].

As ejection and filling do not exactly correspond temporally to sarcomere contraction and relaxation[39], parameters used to study function during systole and diastole will always be influenced by factors beyond underlying cellular function. Notably, differences in loading conditions and heart rate can make it difficult to ascertain what constitutes true differences in underlying diastolic function. A further caveat is that normal cardiac function entails delivering an appropriate cardiac output for the

metabolic needs for the rest of the body. While these needs can vary considerably due to physical activity, diastolic function is most often only assessed at rest, although recommendations for diastolic stress testing have been formulated[40].

2.3.3 Diastolic dysfunction grading *vs.* continuous parameters

Assessment of diastolic dysfunction can be complex. Consequently, a standardized algorithm for assessment as described above is appealing and most likely necessary for clinical practice. However, the algorithms rely on dichotomization of continuous variables, *e.g.,* a cutoff of E/e' > 14. While simplifying algorithm construction, dichotomization of continuous variables inherently leads to loss of information, with loss of statistical power and increased risk of false classification[41]. Also, while diastolic dysfunction grading identifies recognizable phenotypes, it is not clear that progression between grades would be the same across the spectrum of diseases potentially causing diastolic dysfunction, or that the grading would have the same prognostic or treatment implications regardless of the underlying condition. It could therefore be useful to consider using continuous parameters as the basis for informing our clinical and research understanding, rather than using grading based on dichotomization.

2.3.4 The parameterized diastolic filling method

The methods used to study diastolic function as described above, while being founded in physiological reasoning and experimental work, do not constitute an *a priori* formulated framework for studying diastole, but rather a collection of phenomenological observations with different implications for cardiac function and patient prognosis. By contrast, the parameterized diastolic filling (PDF)[42] method applies a kinematic model derived from first principles of physics, firmly positioning the study of early diastolic filling in the broader framework of classical mechanics. The PDF method analyzes early diastolic filling as a result of damped harmonic motion of the LV. Damped harmonic motion describes an oscillatory movement where a damping force decreases the amplitude and speed of the oscillations over time. Figure 3 illustrates this concept graphically. A typical example of damped harmonic motion is the behavior of a spring that is released after having been compressed or extended. The PDF method originated from the realization that the LV, after having been compressed by systolic contraction, behaves much as a recoiling spring during early diastole, and that it should be possible to model this recoiling motion as a damped harmonic oscillator. If mitral valve opening area during the E-wave can be considered constant, PW Doppler of the E-wave will represent the LV expansion or recoil velocity. In other words, LV early diastolic recoil can be modeled as a damped harmonic oscillator with PW Doppler of the E-wave describing the velocity of its motion

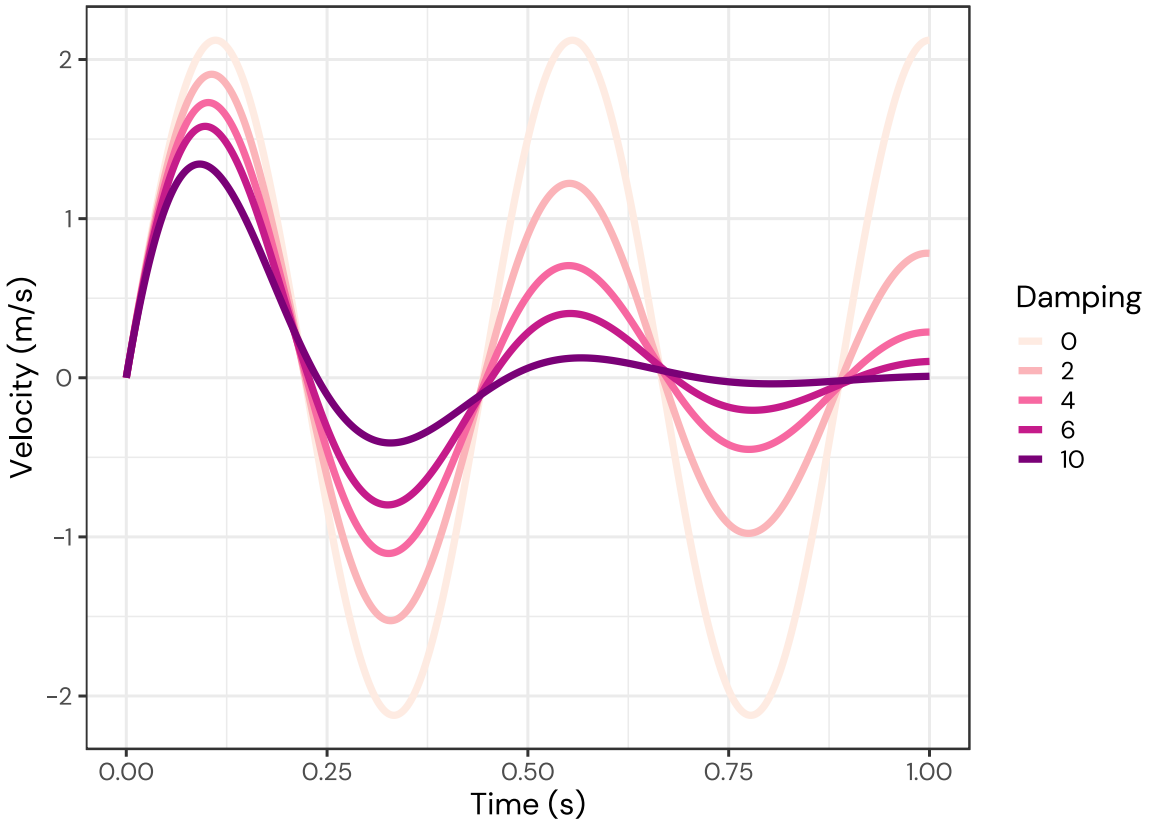

Figure 3. Simple and damped harmonic motion. Illustration of the effect of increasing damping on the velocity of harmonic motion. Damping = 0 illustrates simple (undamped) harmonic motion. Damping values are *c* values, introduced in 2.3.4.1.

2.3.4.1 Damped harmonic motion and derivation of the PDF equations

Damped harmonic motion is an expansion of the concept of simple harmonic motion, in which the driving force *F* is

$$F = -kx, (1)$$

where, taking the analogy of the oscillatory recoiling of a compressed spring, *k* is the stiffness of the spring, and *x* is the displacement (in this case compression) of the spring from its resting length. Stiffness can thus be thought of as an elastic property of the spring, both as it resists compression under force, and as its tendency to recoil to its original state. Expanding on this concept, and noting that Newtonian force can be written as $m\frac{\mathrm{d}^2x}{\mathrm{d}t^2}$, the balance of forces in a damped harmonic oscillator is

$$m\frac{\mathrm{d}^2x}{\mathrm{d}t^2} + c\frac{\mathrm{d}x}{\mathrm{d}t} + kx = 0, (2)$$

where *m* denotes mass with unit g. In the PDF method, mass is set to 1 g, and the other constants are expressed on a per-unit mass basis. The constant *k*, taking the unit N/m or g/s², is the same stiffness constant as in simple harmonic motion (Equation 1), and the constant *c* denotes damping with the unit Ns/m or g/s. The constant *x* indicates the

displacement from equilibrium (*e.g.*, how far a spring has been compressed) in meters. Equation 2 can be restated as an expression of the velocity (v) of motion of the oscillator over time (t) as a function of *k*, *c*, and the amount of displacement at the beginning of motion, x_0. Depending on the relationship between restoring (*k*) and damping factors (*c*), three different solutions for v(t) are found. For underdamped cases, defined by $c^2 - 4k < 0$, the expression is

$$v(t) = \frac{-kx_0}{\omega} * \exp\left(\frac{-c}{2}t\right) * \sin(\omega t), (3)$$

where $\omega = \frac{\sqrt{4k-c^2}}{2}$. (4)

For overdamped cases, defined by $c^2 - 4k > 0$:

$$v(t) = \frac{-kx_0}{\beta} * \exp\left(\frac{-c}{2}t\right) * \sinh(\beta t), (5)$$

where $\beta = \frac{\sqrt{c^2-4k}}{2}$. (6)

For critically damped cases, defined by $c^2 - 4k = 0$:

$$v(t) = -kx_0 t * \exp\left(\frac{-c}{2}t\right). (7)$$

Velocity will decrease asymptotically for overdamped and critically damped cases, as illustrated in Figure 4, contrasting the oscillation of underdamped cases.

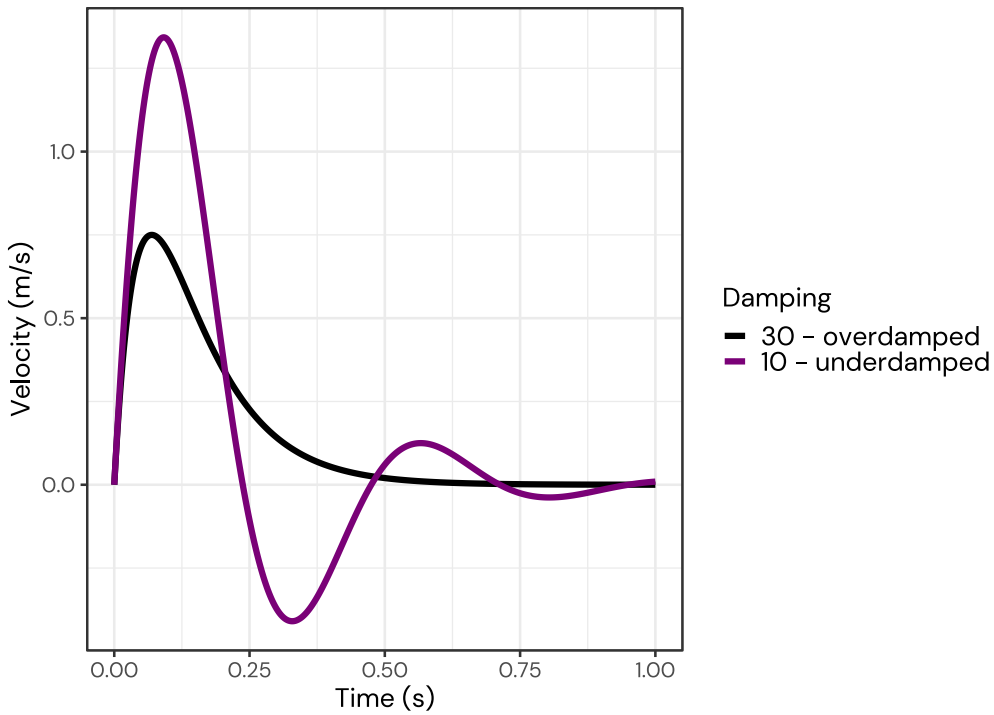

Figure 4. Over- and underdamping. Plot of an underdamped (purple) and overdamped (black) curve. PDF parameters k = 200 g/s², x_0 = -0.15 m, c = 10 and 30 g/s, respectively.

Doppler recordings create plots of velocities over time. The Doppler velocity profile (DVP) is therefore essentially a v(t) graph, and by curve fitting the DVP of early diastolic filling to the PDF equations for v(t), the constants c, k, and x_0 can be obtained for each E-wave. A representative example of a PW Doppler registration of an E-wave with the PDF curve resulting from curve fitting the DVP superimposed is presented in Figure 5.

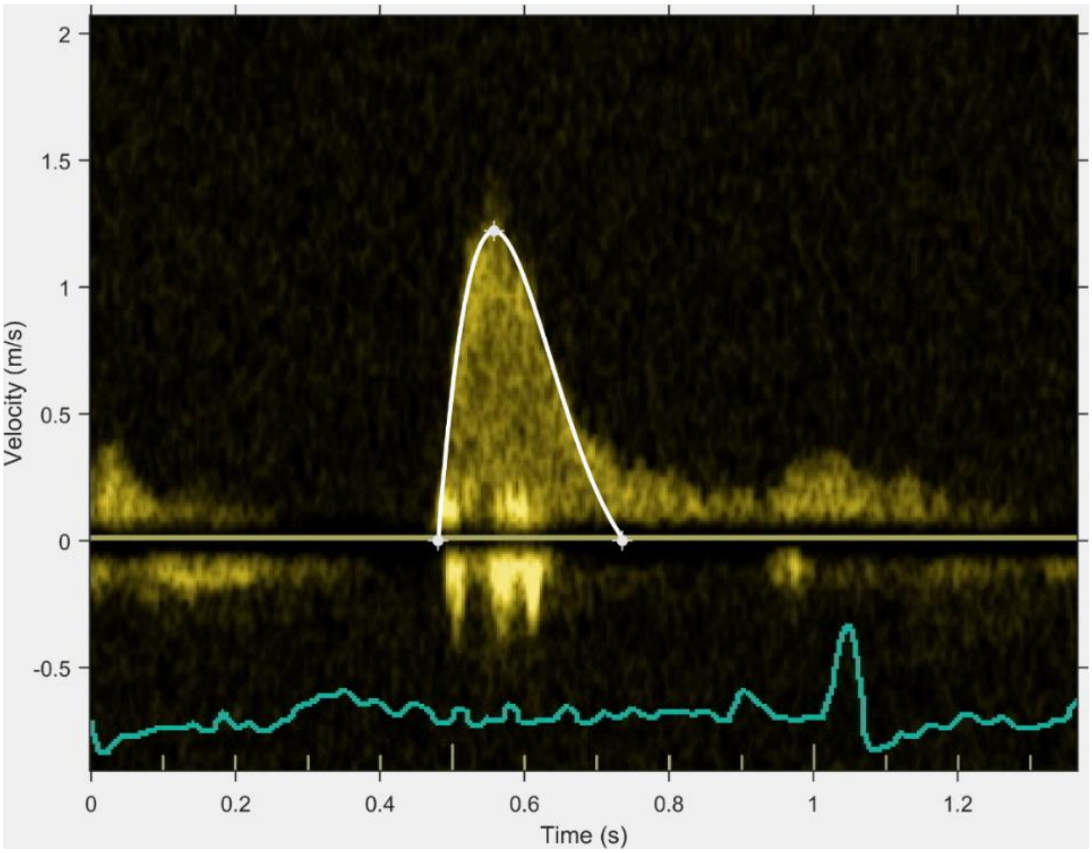

Figure 5. Doppler recording and PDF curve. The white curve was obtained by fitting the Doppler velocity profile to the PDF equation, yielding c = 17.3 g/s, k = 135 g/s², and x_0 = 11.4 cm, and then using these constants to plot v(t) on top of the original image for assessment of fit accuracy.

2.3.4.2 Relationship between overall E-wave shape and the PDF constants

The constants k and c together determine the acceleration time (AT) and deceleration time (DT) of the E-wave. The parameter x_0 is related to the VTI, and thus determines the overall size of the E-wave without affecting AT or DT (VTI = $2x_0$ when c = 0). For a given k and x_0, an increase in c will shorten AT, lengthen DT, and decrease Vmax, and vice versa. For a given c and x_0 an increase in k will shorten AT slightly, shorten DT, and increase Vmax, and vice versa. These effects are demonstrated in Figure 6.

2.3.4.3 Interpretation of the PDF parameters

The three parameters or constants used to describe each E-wave can be interpreted as follows in the application of damped harmonic motion to cardiac diastolic function:

- x_0 – load, the amount of compression of the LV, which is proportional to the volume of blood flow acress the mitral valve during early diastole, and the velocity-time integral of the E-wave.
- k – diastolic stiffness, the tendency of the LV to recoil from its end-systolic compressed state. Compression is expressed in x_0, and the peak driving force of recoil is the product of k and x_0. k has been shown to be linearly correlated to invasively determined stiffness (dP/dt) ($R^2 = 0.71$)[43]. See below for details.
- c – damping, or energy loss, attributed to passive viscoelastic properties of the LV as well as imperfect active relaxation. The peak resistive force of recoil is the product of c and Vmax of the E-wave. The resistive force opposes the driving force, and both are equal at the Vmax of the E-wave.

The parameters load (x_0) and stiffness (k) can at first seem hard to grasp as most cardiologist likely will have thought of load as meaning preload or afterload, and stiffness as a property describing resistance to deformation. This line of thinking is appropriate when considering systolic function. However, early diastole requires focusing on the factors determining recoil, not contraction.

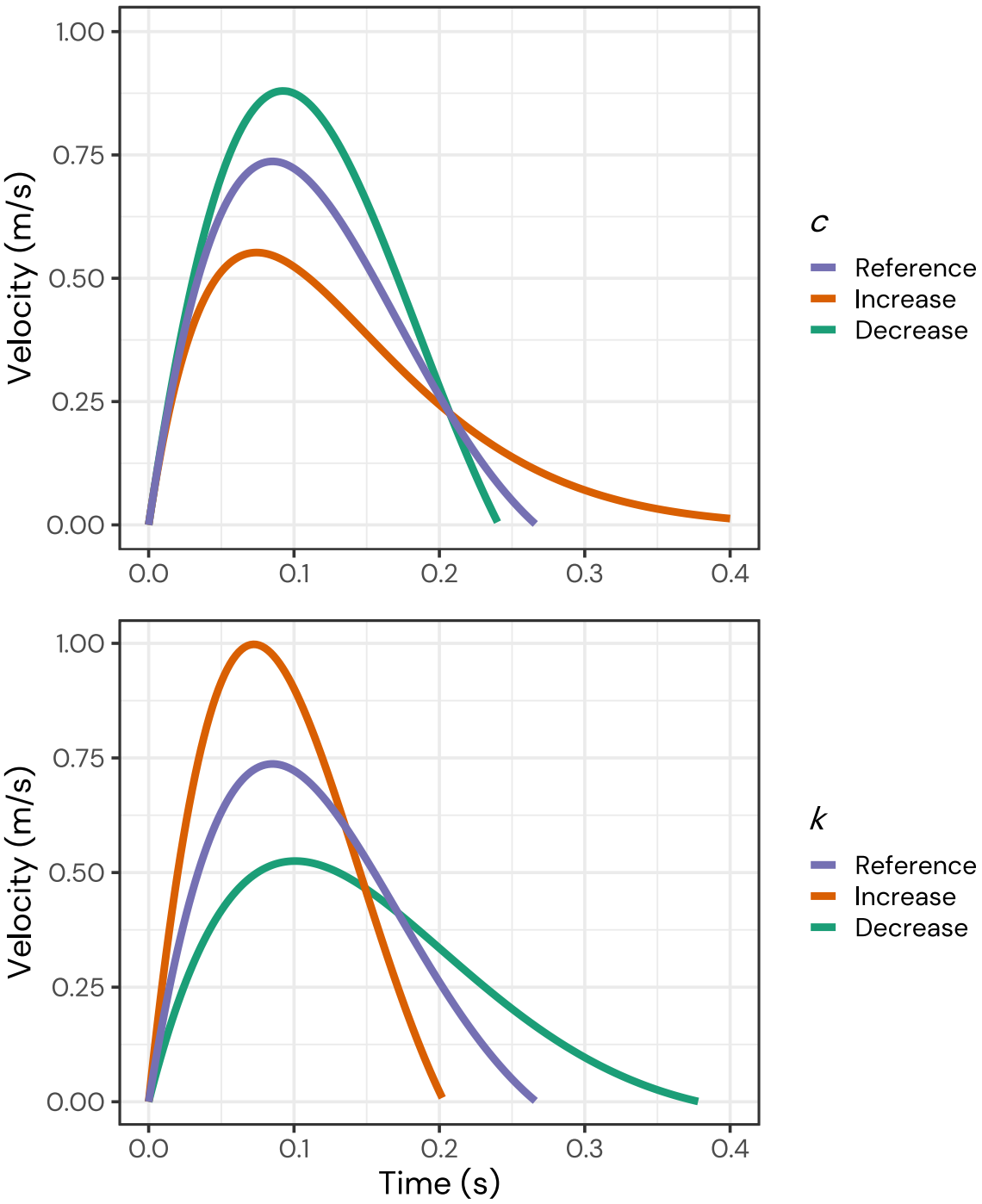

Figure 6. Effect of differences in *c* and *k* on E-wave shape. Reference E-waves are obtained with x_0 = -10 cm, *k* = 195 g/s², and *c* = 15 g/s. Increased *c* = 25 g/s, decreased *c* = 10 g/s. Increased *k* = 295 g/s², decreased *k* = 125 g/s². Other constants held unchanged from reference.

2.3.4.4 Derived PDF parameters

The PDF method expresses each episode of early diastolic filling as a combination of *c*, *k*, and x_0 constants. These constants can be further combined. A direct carryover from classical mechanics is that the stored potential energy at the start of motion is $\frac{1}{2}kx_0$. Exploration of the balance between *c* and *k* have resulted in several derived parameters

of potential physiological interest. The following three arguably have the most potential interest.

1. **The kinematic filling efficiency index**
   After obtaining the basic PDF parameters of an E-wave and calculating the area under the curve (velocity time integral, VTI), a new hypothetical VTI is calculated using the measured k and x_0 values, but setting c to 0. This hypothetical VTI represents the amount of blood that would fill the LV if there was no energy loss during early diastole, and the ratio between measured and hypothetical VTI can be expressed as the kinematic filling efficiency index (KFEI). KFEI has been shown to be reduced in patients with diabetes mellitus[44].
2. **Estimated tau**
   In a fashion similar to KFEI one can calculate how much the DT of the E-wave is prolonged by imperfect relaxation, *i.e.*, damping, by comparing the DT of a measured E-wave with that of an E-wave with the same k and x_0, but with c set to 0. This relaxation component of DT has been shown to be closely linearly correlated with invasively measured tau (R^2 = 0.89)[45], and thus a non-invasively estimated tau can be calculated using a simple linear regression equation.
3. **The load-independent index of diastolic filling**
   In the PDF framework, differences in load are expressed as differences in x. Although the special case of x_0, corresponding to initial load as recoil is about to begin, is used to derive the equations for DVP fitting (equations 3–7), equation 1 holds true for all x_t, meaning x at any time during motion, and the driving force of recoil at a given moment is always kx_t. The driving force will decrease from its peak value of kx_0 (peak driving force) and when passing the timepoint of peak E-wave velocity the resistive forces will be first equal (peak resistive force, cVmax) and then greater than the driving force, and flow velocities start to decrease. Accordingly, at the time of peak E-wave velocity, when there by definition is no acceleration or deceleration, $\frac{\mathrm{d}^2x}{\mathrm{d}t^2} = 0$, and $c\frac{\mathrm{d}x}{\mathrm{d}t} = cVmax$, equation 1 can be restated as $cVmax + kx(t_{peak}) = 0$. It was assumed that the relationship between kx_0 and $kx(t_{peak})$ is linear, and as $kx(t_{peak}) = cVmax$ at peak velocity, the equation $kx_0 = M * cVmax + B$ can be formulated. This implies that the relationship between peak driving force and peak resistive force is linear, and that the slope (M) of the relationship will be constant despite varying load, thus being a load independent index of diastolic filling. The linearity and load independence of the relationship was also demonstrated empirically with load manipulated with a tilt board. The interpretation of M, although not thoroughly investigated in diverse clinical settings, is somewhat similar to KFEI and tau, as lower M values imply higher resistive forces due to inefficient conversion of potential to kinetic energy.

M has been found to be lower in patients with increased LV filling pressure when compared to controls[46].

2.3.4.5 Validation of the PDF method

Validation of the PDF model in the sense that curves produced with equations 3–7 accurately describe E-waves have been demonstrated in several studies[42,47–50,46,44]. It has been demonstrated on a beat for beat basis that the PDF stiffness parameter *k* has a high degree of correlation with invasively measured LV stiffness, as predicted by the model[43]. Measurement of viscoelasticity *in vivo* is challenging[51] and such validation of the PDF parameter *c* has not been performed. However, as noted above, the predicted relationship between tau and how *c* lengthens DT has been demonstrated invasively[45].

2.3.4.6 "Ringing" of the LV

The PDF equation for the underdamped case predicts an oscillatory motion with decreasing amplitude. Noting that the model only predicts the effect of early diastolic recoil of the LV, and not the totality of diastole, the first negative oscillation would in many cases come clearly before the A-wave (*e.g.*, the underdamped curve in Figure 2). While a reversal of blood flow from the LV to the LA is not clinically recognized, oscillations of the mitral ring, which can move around a column of blood, have been noted[52], and the PDF equations have been fitted to TDI registrations showing agreement between predicted oscillations and observed TDI signal with a positive wave after e'[53].

2.3.4.7 Limitations of the PDF method

The PDF method has not been extensively applied, likely due to its somewhat technical nature. Compared to more commonly applied methods to diagnose diastolic dysfunction, there is a paucity of data regarding the prognostic utility of the method, with one exception being a small study where $c^2 - 4k$ was found to have prognostic value with values < -900 indicating a 1-year mortality risk of almost 50%[49].

By definition, the PDF method only models diastolic filling that is a result of LV recoil. It is not uncommon to have PW Doppler signal of blood flow during diastasis, and regardless of whether this is transmitral blood flow caused by pulmonary venous inflow increasing left atrial pressure[54] or an effect of subvalvular vortex formation[55], these aspects of diastole are not addressed in the PDF model. For an example, see Figure 7. The original description of the model included modeling of the A-wave[42], but this has seemingly not been explored or validated further. How to integrate PDF results with other methods, *e.g.*, tissue Doppler, also remains to be explored.

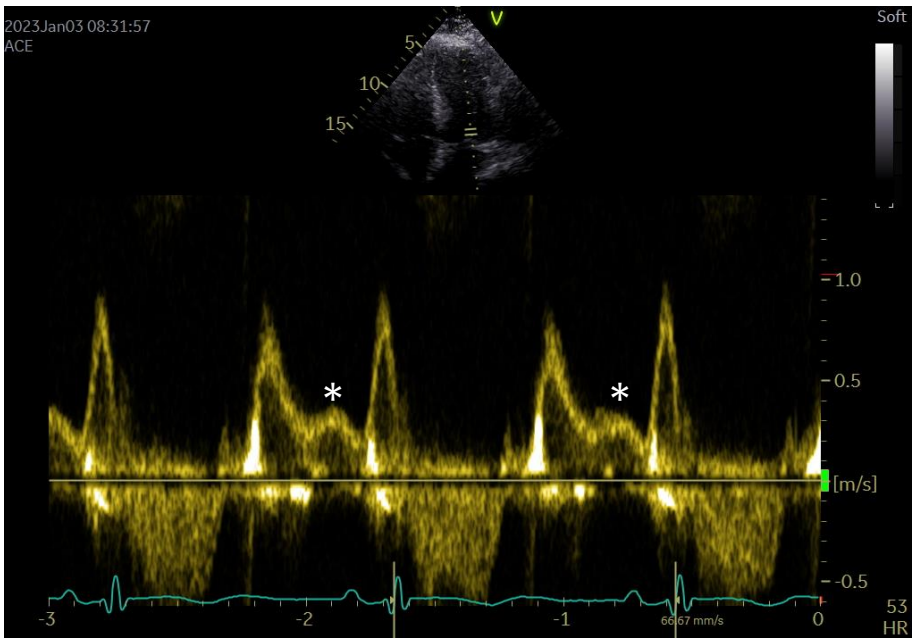

Figure 7. PW Doppler of mitral inflow with prominent L-waves marked with asterisks. The L-waves cannot be analyzed by the PDF method.

Finally, the PDF method is a so-called lumped parameter model, meaning that it is limited to the constants c, k, and x_0. These constants correspond to damping, stiffness, and load, respectively. Any phenomenon that affects the shape of the DVP in the same way as a change in for instance myocardial stiffness would, will be lumped in the constant k. The same applies to differences in c and x_0. This means that the PDF parameters have not been shown to be specific to a singular pathophysiological process, but rather reflect the composite net consequence of multiple potential pathophysiological mechanisms.

2.4 Diastolic function during myocardial ischemia and after myocardial infarction

The effect of myocardial ischemia on diastolic function was initially studied invasively in dogs and humans, finding increased stiffness in humans shortly after acute MI[56,57] but decreased stiffness in dogs in experimental MI[58]. These studies did not study relaxation, which was later found to be impaired in a time-varying manner, as well as preceding systolic dysfunction when measurements were done at the onset of ischemia[59,60]. Studies using PW Doppler assessment of diastolic function found indications of reduced filling with impaired relaxation during coronary occlusion[61,62], but also decreased total flow replicating some earlier invasive findings[63]. Notably, these studies were small, typically enrolling approximately 20 patients each. Furthermore, and perhaps more pertinently, no method for quantifying the extent of myocardial ischemia was used.

Rather, myocardial ischemia was considered either as an either–or phenomenon, and sometimes its effect was studied dynamically over a brief period of time.

It has been demonstrated that a restrictive filling pattern, indicating elevated filling pressures, is a marker of poor prognosis[64,65], but what causes some patients to develop this pattern is not widely studied. With the advent of IS quantification using SPECT and CMR, the severity of myocardial ischemic damage quantified as IS can be used to study how the extent of MI affects diastolic function. As per section 2.3.3, this also allows MI to be treated as a continuous variable, retaining maximum information. There exists a body of literature using blood biomarkers such as troponins and CK-MB as proxies for IS. However, considering the sometimes modest correlation between these biomarkers and IS in real-life clinical settings[66], studies based on quantification of IS using blood biomarkers will not be explored further here. Instead, the focus will be on results using imaging methods to quantify IS.

Early studies that did not employ TDI or diastolic dysfunction grading typically found a modest correlation between IS and increased E-wave velocity and diverging results regarding DT in patients shortly after MI or with chronic LV dysfunction due to ischemic heart disease[67,68], suggestive of both increased stiffness and increased filling pressures. Later studies incorporating TDI have found a weak negative correlation between IS and e′, and similarly weak correlations with increasing E/A ratio and decreasing DT[69]. Some studies also examined IS in relation to diastolic dysfunction grade, although with grading performed using varying grading algorithms, making it difficult to compare across studies[69,70].

Although identifiable and quantifiable by CMR, the role of myocardial edema in this setting has not been extensively studied. One study using only CMR found a moderate correlation between regional T1 values and circumferential diastolic strain rate from tagging sequence images[71], and two studies with diastolic function assessed by echocardiography found small[70] or no[72] effect of myocardial edema using conventional parameters. No previous studies have used the PDF method to determine the relationship between diastolic function and myocardial edema or infarction.

2.5 Echocardiography and CMR in MINOCA

MINOCA as a working diagnosis by definition implies a need for further investigations. CMR can identify convincing evidence supporting different final diagnoses. The ability of CMR to differentiate between different causes of myocardial injury is appealing and has led to its wide recommendation[24,26]. While the addition of OCT to coronary angiography has gained interest[73–75], the role of echocardiography in this setting has not been studied. Echocardiography, which in stark contrast to CMR is widely available, could potentially have a role in identifying those patients with MINOCA as a working diagnosis where further investigations are futile, especially when combined with other information

such as blood biomarkers of myocardial injury (hs-TnT) or increased filling pressures (NT-pro-BNP).

3 Research aims

The overall aim of the doctoral project was to evaluate echocardiographic methods in myocardial infarction patients using cardiovascular magnetic resonance imaging as a reference. The ambition to use to the PDF method led to the development of an improved tool for its application, and a realization of the need for reference values for the method.

The specific aims were:

Study I

To develop a software tool facilitating the analysis of diastolic function with the PDF method, and as a secondary aim to assess the inter- and intraobserver reliability of the PDF method using this tool.

Study II

To describe normal reference values for the PDF parameters.

Study III

To study the relationship between quantitative measures of myocardial injury by CMR including IS and MaR, and different quantitative measures of diastolic function. The hypothesis was that IS and MaR both have a negative impact on diastolic function.

Study IV

To study the potential of echocardiography, NT-pro-BNP, and hs-TnT as gatekeepers for further evaluation by CMR in patients with MINOCA. The hypothesis was that patients with a normal echocardiogram would not receive a diagnosis by CMR.

4 Materials and methods

4.1 Ethical considerations

The patient material in this thesis is derived from two clinical trials (Studies I, III, and IV), and a pre-existing database (Study II). The randomized RECOND trial[76] (Studies I and III) was approved by the Regional Ethical Review Board in Stockholm with approval number 2013/385-31/1, and the diagnostic SMINC2 study[27] (Study IV) with approval number 2014/131-31/1. Use of the database used in Study II was approved by the Singhealth Centralised Institutional Review Board (CIRB Ref 2016/3163). This thesis comprises echocardiographic substudies where patients were not exposed to additional risk as a result of their participation in the substudies, and a retrospective analysis of data similarly not affecting patient risk of harm.

All data were anonymized before statistical analysis, and no information was used in presentation of the results that could lead to identification of individual patients. Study participants were exposed to minimal risk, and the results could be of potential benefit for future patients.

4.2 Study I

4.2.1 Design

Study I comprised the description of a software application that was developed as a part of this thesis, and the analysis of inter- and intraobserver reliability of the PDF method using the finished application.

4.2.1.1 Development of the software application

The application, subsequently published under the name Echo E-waves, was developed using the MATLAB® programming language and platform, with additional code in the Java language. MATLAB was chosen for its native support for reading files in the digital imaging and communications in medicine (DICOM) format, and ease of building graphical user interfaces. Open-source alternatives such as R or Python did not, at least at the start of the project, offer equivalent solutions. Key features of the application and considerations made during implementation include:

- *Utilization of DICOM metadata*. A DICOM file contains an image or series of images either as a stack or a movie, and a header consisting of metadata ("tags") describing the contents of the file and various characteristics of the data. The application uses the metadata to verify that the data contained is PW Doppler, and applies the contained scaling information to properly set the time and velocity scales, and find the baseline representing 0 velocity for the image as it is displayed in the graphical user interface.

- *Velocity profile detection*. A key point in utilizing the PDF method is to decide which data to fit to the damped harmonic motion equation. The PW Doppler image contains an abundance of non-zero data so fully automated methods using metrics such as sum of squared errors or R^2 for curve fitting will result in poor visual agreement with what is commonly understood as the DVP of the E-wave. The guidelines[77] recommend that traces of the velocity profile should be performed at the "outer edge of modal" velocity. However, the true modal velocity in the mathematical sense, and therefore the most easily implementable algorithmically, is the most commonly occurring velocity at each timepoint. This mode is invariably located at the central and brightest part of the velocity profile, and does not have an outer edge *per se*. The outer edge that is recognizable and used by trained clinicians lacks a mathematical definition, but empirically seems to correspond to velocities at approximately 85% of the signal intensity of the true modal velocity. After trying different methods, the most robust algorithm consisted of searching each image column (*i.e.*, time point in the data) for the highest velocity having a Doppler signal intensity above an empirically set cut-off value. The cut-off value can be changed in order to find the value giving the best identification of the DVP. The algorithm also tries to filter noise by excluding velocities that constitute large deviations from velocity of the preceding time point, instead interpolating a velocity in its place. The algorithm is applied on a segment of the DICOM image identified by the user, clicking and dragging with the mouse from the start of the E-wave to where it either ends, or is obscured by interfering signal. An additional challenge is that the DICOM image contains Doppler signal data that is not part of the E-wave, but also signal from mitral valve motion, noise, and most importantly blood flow that is not directly generated by the recoil of the LV. As the PDF method only models the recoil-driven part of diastole, only Doppler signal deemed to be caused by this phenomenon should be fitted to the function. These problems typically occur during the end of E-wave and can be alleviated by either fitting less than the whole duration of the E-wave or by interpolating a straight-line tangent during the latter half of the DT, as in clinical echocardiography.
- *Visual feedback of curve fitting*. The PDF curve resulting from curve fitting is directly superimposed on the DICOM image facilitating assessment of fit accuracy. Modifications are directly updated.
- *Semiautomatic curve fitting*. In order to facilitate faster fitting of larger sets of E-waves, and potentially reducing observer variability, a semiautomatic fitting algorithm was implemented. Although one can expect consecutive E-waves from a patient to be fairly similar, and therefore use this similarity to guide fitting, the automatic identification of where the E-wave is temporally located in the DICOM image is of utmost importance. This is because the DVP identification algorithm

is naïve to where it is being applied. This was solved by using the first milliseconds of an E-wave that the user has manually fitted, and using this image fragment as a template for finding the start of the other E-waves. The rationale for this was that start of the E-wave including the mitral valve artifact seem to be fairly stereotypic and reproducible. Using normalized cross-correlation, a method which matches the correlation of two signals as a function of their temporal offset, the application can identidy the start of the E-waves with seemingly high accuracy. Using the combination of normalized cross-correlation of E-wave onset, and the DVP identification algorithm, it is possible to rapidly fit large sets of E-waves.

- *Geometric method.* As described by Shmuylovich[78], each combination of c, k, and x_0 yields a unique combination of AT, DT, and Vmax, and *vice versa*. The method has been implemented in the application so that the user can mark the beginning, peak and end of an E-wave, and the corresponding PDF curve will be plotted. The three points can also be dragged with instantaneous update of the plotted curve. Notably, this method only uses three measurements from the actual data, as opposed to curve fitting the actual DVP, and requires close attention to agreement between the E-wave and PDF curve.
- *Quality control.* The interface facilitates review of fitted E-waves by displaying each fit in a list, in a plot of all PDF curves, and as point in a scatter plot of kx_0 vs cVmax. Selecting the E-wave in any of these three display formats will retrieve the Doppler image with its superimposed PDF curve.
- *Data export.* Data can be stored and exported in MATLAB:s .mat format, containing all images and PDF fitting results, making it possible to review completed analyses and collaborate with other investigators. Additionaly, the PDF results can be stored to the computer's clipboard, or by generating an Excel® file containing the data. It is also possible to assign a folder for several runs of analysis, in this case the application will append data to a common Excel file, essentially creating a database.

4.2.2 Data sources and measurements

Ten patients each from the RECOND[76] and SMINC2[27] studies were non-randomly selected on the basis of having moderate to good quality PW Doppler DICOM images of transmitral flow, as assessed by the first author. In both studies, the recordings of transmitral flow were performed during shallow free breathing for the time necessary to fill a screen width of data at a sweep speed of 12.5 mm/s, approximately 16 seconds. Recording during free breathing was performed twice, and two similar recordings were also performed after the performance of the Valsalva maneuver. At the time of analysis, the Doppler data was displayed at a sweep speed of 100 cm/s. The Echo E-waves application was used to perform all PDF analysis.

4.2.3 Statistical methods

The PDF parameters were presented as median values with total and interquartile ranges (IQR). Inter- and intraobserver reliability was assessed using the intraclass coefficient of variation (ICC, two-way random effects model for agreement on per-patient averages), and the coefficient of variation (CV) calculated as the standard deviation of the mean differences between analyses divided by their means and expressed as a percent, and the percentage difference between measurements. All statistical analyses were performed in MATLAB release 2015a (Mathworks, Natick, Massachusetts, USA).

4.3 Study II

4.3.1 Design

This was a retrospective analysis of an existing database to identify patients with a high likelihood of absence of significant cardiovascular or related disease, in order to establish normal reference values for the PDF method. Patients were excluded on the basis of pathological results on stress echocardiography, as well as abnormal left atrial or LV volumes, or hypertrophy of the interventricular septum as per guidelines[79]. Likewise, patients with preexisting diabetes mellitus, hypertension, atrial fibrillation, or suboptimal PW Doppler images of transmitral flow were excluded.

4.3.2 Data sources and measurements

The National Heart Centre in Singapore hosts a comprehensive database of outpatient resting and stress echocardiography results. The database also contains relevant information on comorbidities, as completed on a clerking proforma for all patients by an attending physician. The database was made available in a collaboration between the Karolinska Institute and the National Heart Centre. Conventional echocardiographic parameters were extracted from the database, and PDF analysis was performed on exported DICOM images using the Echo E-waves application, on one E-wave per patient.

4.3.3 Statistical analysis

The normal reference values were presented as means and the interval between the 2.5th and 97.5th percentiles. Differences between men and women were analyzed using Student's t-test or the Mann-Whitney U-test, after statistical normality was assessed using a combination of visual inspection of histograms and the Kolmogorov-Smirnov test. Correlations between the PDF parameters and systolic and diastolic blood pressure and age, respectively, were assessed using Pearson's r. ICC was used to investigate intraobserver variability in 20 patients. A p-value of less than 0.05 was

considered statistically significant. All statistical analyses were performed in MATLAB release 2015a (Mathworks, Natick, Massachusetts, USA).

4.4 Study III

4.4.1 Design

This was a preplanned echocardiographic substudy of the RECOND[76] trial. The purpose of the study was to examine how IS and the myocardial edema of the MaR influence the parameters used to assess diastolic function, both conventionally and in the PDF framework. In RECOND trial, patients underwent CMR 4-7 days and 6 months after MI, with echocardiography performed within 24 hours and two weeks of CMR, respectively. Patients undergoing primary PCI for anterior STEMI were eligible for inclusion. Exclusion criteria included age under 18 years, previous MI, previous coronary artery bypass grafting, severe peripheral arterial disease, atrial fibrillation, treatment with glibenclamide or cyclosporine, and cardiac arrest, as well as standard exclusion criteria for CMR such claustrophobia and incompatible implanted ferromagnetic objects. The hypothesis of the RECOND trial was that remote ischemic conditioning would increase the myocardial salvage index (difference between MaR and IS, divided by MaR), but no evidence was found for this.

4.4.2 Data sources and measurements

In the acute setting, 74 patients underwent echocardiography the same day as CMR. At 6 months, 61 patients had a follow-up echocardiographic examination. Relevant CMR measurements were taken from the original analyses for the RECOND trial. Conventional echocardiographic analysis was performed in accordance with clinical guidelines[77,79] using EchoPAC v1.13 (General Electric Healthcare, Horten, Norway) by the first author of the study, and PDF analysis was performed using the Echo E-waves application. The manner in which E-waves were recorded during echocardiography is described in section 4.2.2.

4.4.3 Statistical analysis

As, the distributions of the analyzed parameters were a mix of normal and non-normal, all parameters were reported as medians and IQRs. The relationship between the IS, MaR, and the diastolic parameters were modeled using linear regression with three-knot restricted cubic splines without further testing of fit optimization. This approach was chosen as it would accommodate non-linear relationships without engaging in data-driven overfitting[80]. Every diastolic parameter was modeled first using only IS as independent variable, and then using IS and MaR. The models were then compared with using a likelihood ratio test to analyze if the addition of MaR improved goodness of fit. For the follow up examinations, the diastolic parameters were modeled using IS at 6 months. Statistical analysis was performed in R v4.1.3 (R Core Team, 2021)[81].

4.5 Study IV

4.5.1 Design

This was a preplanned substudy of the SMINC2[27] study, investigating to what extent MINOCA patients with normal echocardiographic examinations, or low levels of hs-TnT and NT-pro-BNP, receive a final diagnosis using CMR. As it pertains to Study IV, patients in the SMINC2 trial were examined with CMR and echocardiography on the same day, after being included on the grounds of having suspected MINOCA after having made a clinical presentation as an ACS, and subsequently undergoing invasive coronary angiography. Exclusion criteria were age below 35 or over 69 years, non-sinus rhythm, pulmonary embolism, severe chronic obstructive pulmonary disease, previous MI, known cardiomyopathy, serum creatinine < 150 µmol/L, presence of a pacemaker, and claustrophobia. The hypothesis of the SMINC2 study was that > 70% of patients would receive a diagnosis using early comprehensive CMR. The study showed that this was achieved in 77% of patients.

For Study IV, diagnosis by CMR was considered the reference standard, and a normal echocardiographic examination was defined as LVEF ≥ 55%, global longitudinal strain ≥ 17 %, E/e' ≤ 14, and absence of RWMA, including assessment after intravenous contrast (SonoVue®, Bracco) administration.

4.5.2 Data sources and measurements

CMR was performed at a median of 3 [IQR 2–4] days after hospital admission. Same day echocardiography and CMR was available in 128 patients. Five patients were excluded based on readily identifiable cardiomyopathy on echocardiography, although verified by CMR, as these were considered not reflective of MINOCA patients where the comparative value of CMR is uncertain. Final diagnosis, which was defined by CMR, was taken from the SMINC2 study. All echocardiographic measurements were performed in EchoPAC 2.03 (General Electric Healthcare, Horten, Norway) by the first author. Levels of hs-TnT and NT-pro-BNP was analyzed in blood drawn on the same day as CMR.

4.5.3 Statistical analysis

For the calculation of sensitivity, specificity, positive and negative predictive value (PPV and NPV, respectively), and positive and negative likelihood ratios, a pathological echo was considered as a positive test and the presence of any diagnosis by CMR as a positive case. The relationship between the levels of hs-TnT and NT-pro-BNP and establishing a diagnosis by CMR was assessed in the following manner. First, logistic regression models with the respective biomarker level as independent variable and presence of any CMR diagnosis as a binary dependent variable were fitted. These models were then used to predict how the probability of establishing a diagnosis increases with increasing biomarker levels, by converting the log odds to probabilities.

As these predictions were produced to give a rough estimate of the magnitude of the probabilities, no further model optimization was attempted. All statistical analyses were performed in R version 4.1.2 (R Core Team, 2021)[81].

5 Results

5.1 Study I

The finished software application was made available for free at the website www.echoewaves.org. The distribution of the PDF parameters in the 20 examined patients are presented in Table 1. For each patient a median of 34 (IQR: 29-42) E-waves were analyzed, using the automatic fitting method of the application, followed by manual revision of curve fitting, if necessary. The results of intra- and interobserver reliability analysis is presented in Table 2. With the exception of M and B, inter- and intraobserver agreement was good or excellent. As the observers had not applied the PDF method on the exact same E-waves for each patient, likely due to differences in assessment of Doppler quality, statistical analysis was done on both per-patient averages of the slightly diverging E-wave sets (Table 2a), and averages of the exact same E-waves per patient (2b), with similar results. The average time spent on analysis was 7.6 seconds per E-wave, including automatic fitting and review. The layout of the graphical user interface is illustrated in Figure 8.

Table 1. Distribution of PDF parameters.

Parameter	Median	Range	IQR
c, g/s	17.4	10.6–32.8	15.5–20.4
k, g/s²	177.4	106.5–294.8	153.9–206.9
x_0, cm	11.7	7.7–17.9	10.3–12.8
Vmax, m/s	0.7	0.5–1.3	0.6–0.8
Edec. ms	236	139–473	205–273
VTI, cm	12.4	8.1–19.1	11.0–13.5
Tau, ms	70.1	47.6–151.6	62.0–83.3
KFEI, %	53.0	46.1–64.1	51.4–54.8
$c^2 - 4k$, g²/s²	-382	-826–224	-474–-295
Filling energy, mJ	1.1	0.6–3.3	0.9–1.4
Peak DF, mN	19.6	12.4–40.6	17.6–22.7
Peak RF, mN	12.5	7.6–27.4	10.6–14.7
M, dimensionless	1.17	0.96–1.49	1.06–1.26
B, mN	5.3	1.6–9.7	4.1–6.7

DF – driving force. Edec – E-wave deceleration time. KFEI – kinematic filling efficiency index. RF – resistive force. Vmax – maximum velocity. VTI – velocity time integral.

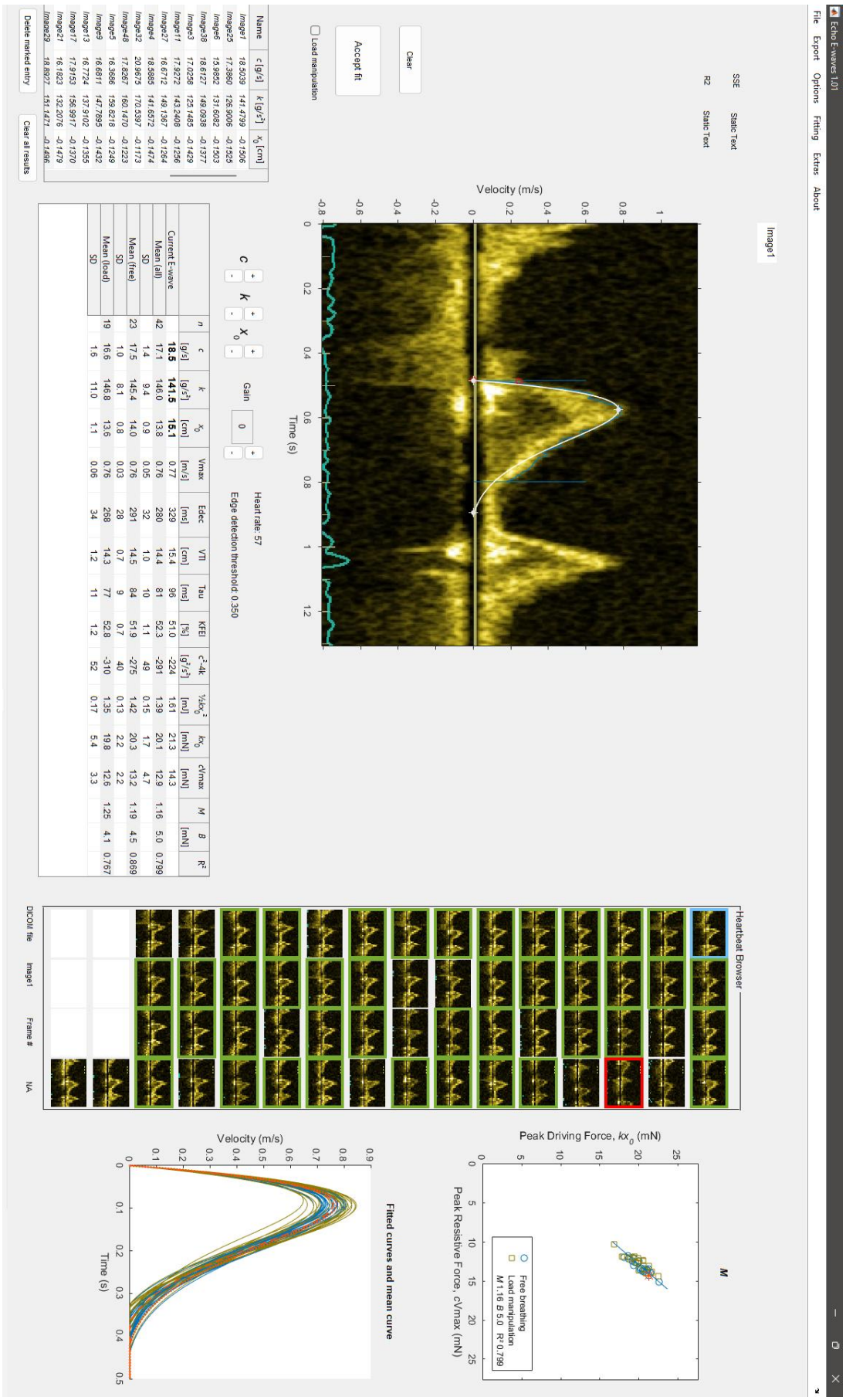

Figure 8. The Echo E-waves graphical user interface.

Table 2. Intra- and interobserver reliability analysis.

	Intraobserver				Interobserver			
2a	CV	Difference	SD	ICC	CV	Difference	SD	ICC
c, g/s	13.2	12.6	9.8	0.80	11.6	9.8	6.1	0.92
k, g/s²	9.3	9.1	7.3	0.93	14.0	9.0	8.3	0.88
x_0, cm	6.6	4.7	4.8	0.95	5.9	4.7	4.6	0.96
Vmax, m/s	5.1	3.3	4.0	0.98	4.0	3.0	2.6	0.99
Edec. ms	11.1	7.6	7.5	0.92	11.8	9.1	6.2	0.93
VTI, cm	6.0	4.1	4.2	0.96	5.3	4.3	3.4	0.97
Tau, ms	11.7	8.9	8.4	0.88	13.3	10.2	6.7	0.91
KFEI, %	2.7	2.6	2.0	0.89	2.5	2.2	1.9	0.91
$c^2 - 4k$, g²/s²	-18.7	-18.9	30.1	0.92	-14.3	-16.2	14.7	0.95
Filling energy, mJ	14.6	13.7	9.6	0.94	10.6	9.8	6.4	0.98
Peak DF, mN	10.7	9.8	8.1	0.92	10.6	8.1	6.0	0.95
Peak RF, mN	14.6	13.5	10.6	0.85	12.9	10.6	7.2	0.93
M, dimensionless	15.3	12.1	8.3	0.51	23.7	17.7	20.8	0.16
B, mN	50.8	45.0	36.4	0.17	51.9	40.4	39.5	0.37

	Intraobserver				Interobserver			
2b	CV	Difference	SD	ICC	CV	Difference	SD	ICC
c, g/s	13.6	12.5	10.6	0.80	11.6	10.4	5.3	0.93
k, g/s²	9.0	8.6	6.8	0.94	13.7	9.2	7.7	0.88
x_0, cm	5.5	3.9	4.8	0.96	5.5	4.3	4.5	0.96
Vmax, m/s	2.4	2.3	1.9	0.99	3.8	3.0	2.5	0.99
Edec. ms	9.7	6.9	7.1	0.94	11.5	7.9	6.6	0.94
VTI, cm	4.0	2.9	3.1	0.98	5.1	4.2	3.2	0.97
Tau, ms	10.7	8.6	8.0	0.90	13.1	8.8	7.1	0.92
KFEI, %	2.9	2.6	2.3	0.88	2.6	2.4	1.8	0.91
$c^2 - 4k$, g²/s²	-17.9	-15.8	25.0	0.93	-12.7	-13.1	11.9	0.96
Filling energy, mJ	16.0	14.2	11.0	0.93	10.9	9.7	6.5	0.98
Peak DF, mN	11.0	10.5	8.5	0.91	10.8	8.2	5.9	0.94
Peak RF, mN	15.7	14.5	11.8	0.83	13.3	10.9	6.9	0.93
M, dimensionless	15.4	12.1	8.3	0.61	13.5	10.2	11.2	0.71
B, mN	44.7	39.5	32.6	0.51	27.9	19.6	19.9	0.83

2a – results with individual selection of E-waves for analysis. 2b – results with same selection of E-waves. DF – driving force. Edec – E-wave deceleration time. KFEI – kinematic filling efficiency index. RF – resistive force. Vmax – maximum velocity. VTI – velocity time integral.

5.2 Study II

The available database consisted of 726 patients. Of these, 138 (19%) fulfilled the inclusion criteria and had transmitral PW Doppler images of sufficient quality for PDF analysis. The mean age was 47 years (95% limits: 27-70 years), and 45% were women. The PDF results are presented as means and 95% limits in Table 3 and graphically in Figure 5, including comparisons between women and men. Women had higher c and k values than men (17.9 [11.6–25.8] vs 15.6 [10.2–23.4] g/s, $p < 0.001$ and 207 [110–303] vs 182 [116–274] g/s^2, $p < 0.001$, respectively), which also was the case for the derived parameters KFEI, filling energy, and peak driving and peak resistive forces (data in Table 3). Furthermore, correlations between the parameters and age, and systolic and diastolic blood pressure are presented in Table 4. The only statistically significant correlations were between systolic blood pressure and k ($r = 0.24$, $p = 0.04$), and between diastolic blood pressure and x_0 and filling energy ($r = -0.27$, $p = 0.02$; $r = -0.29$, $p = 0.01$). Age was not correlated with the PDF parameters.

Table 3. Normal values for the PDF method.

	All (n = 138)		Men (n = 76)		Women (n = 62)		
Parameter	Mean	95% limits	Mean	95% limits	Mean	95% limits	p-value
c, g/s	16.6	10.2–25.3	15.6	10.2–23.4	17.9	11.6–25.8	<0.001
k, g/s²	193	115–295	182	116–274	207	110–303	0.001
x_0, cm	10.4	6.3–14.4	10.3	5.7–14.8	10.7	7.0–14.4	0.30
$c^2 - 4k$, g²/s²	-484	-801—-243	-474	-827—-246	-495	-794—-240	0.40
Tau, ms	64	48–91	63	48–88	65	52–96	0.21
KFEI, %	55	51–63	56	51–64	54	51–59	0.04
Filling energy, mJ	1.07	0.40–2.18	0.97	0.41–1.82	1.21	0.38–2.33	0.01
Peak DF, mN	19.9	11.5–31.7	18.3	11.4–26.8	21.9	11.5–37.0	<0.001
Peak RF, mN	11.9	6.2–20.4	10.8	6.3–16.8	13.4	6.2–22.8	<0.001

DF – driving force. KFEI – kinematic filling efficiency index. RF – resistive force.

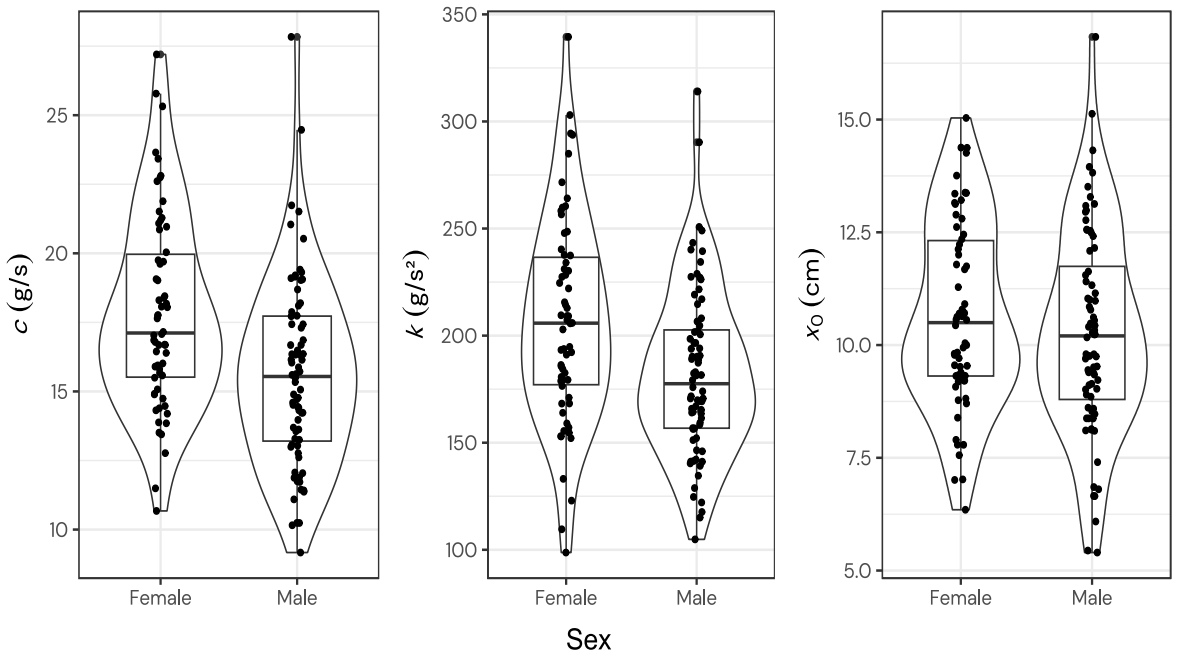

Figure 5. Distributions of *c*, *k*, and x_0 in men and women.

Table 4. Correlations with age (A) and blood pressure (B).

A	All		Men		Women	
	r	p	r	p	r	p
c, g/s	0.16	0.06	0.18	0.12	0.01	0.95
k, g/s²	0.12	0.18	0.12	0.28	0	0.99
x_0, cm	-0.13	0.13	-0.09	0.43	-0.23	0.07
$c^2 - 4k$, g²/s²	0.01	0.88	0.03	0.82	0.03	0.80
Tau, ms	0.12	0.18	0.18	0.13	0	0.99
KFEI, %	-0.08	0.34	-0.08	0.50	0.04	0.78
Filling energy, mJ	-0.08	0.33	-0.07	0.57	-0.22	0.09
Peak DF, mN	-0.02	0.82	0	> 0.99	-0.18	0.17
Peak RF, mN	0.02	0.85	0.05	0.66	-0.16	0.23

B	All				Men				Women			
	SBP		DBP		SBP		DBP		SBP		DBP	
	r	p	r	p	r	p	r	p	r	p	r	p
c, g/s	-0.03	0.76	-0.06	0.52	0.15	0.19	0.11	0.35	-0.11	0.41	-0.07	0.60
k, g/s²	0.06	0.49	-0.07	0.44	**0.24**	**0.04**	0.09	0.45	0	0.98	-0.08	0.54
x_0, cm	-0.04	0.63	-0.06	0.47	-0.19	0.10	**-0.27**	**0.02**	0.12	0.37	0.21	0.10
$c^2 - 4k$, g²/s²	-0.1	0.23	0.04	0.68	-0.14	0.24	< 0.01	>0.99	-0.1	0.46	0.04	0.77
Tau, ms	-0.06	0.48	0	0.96	0.02	0.90	0.05	0.67	-0.14	0.27	-0.02	0.87
KFEI, %	0.07	0.40	0.01	0.93	-0.01	0.92	-0.07	0.52	0.12	0.34	-0.02	0.88
Filling energy, mJ	-0.01	0.94	-0.10	0.24	-0.12	0.29	**-0.29**	**0.01**	0.12	0.38	0.14	0.29
Peak DF, mN	0.02	0.78	-0.10	0.26	0.01	0.91	-0.2	0.09	0.09	0.47	0.09	0.48
Peak RF, mN	0	0.96	-0.09	0.31	0.02	0.89	-0.13	0.26	0.05	0.70	0.08	0.55

DBP – diastolic blood pressure. DF – driving force. KFEI – kinematic filling efficiency index. RF – resistive force. SBP – systolic blood pressure.

5.3 Study III

Out of 93 patients included in the RECOND trial, 74 had an echocardiographic examination performed within 1 [IQR 0–1] days of the first CMR examination, which in turn was performed 4–7 days after PCI. At 6 months follow-up, echocardiography was available in 61 patients. Patient characteristics and CMR findings are presented in Table 5. The distributions of IS and MaR are presented in Figure 6, illustrating their wide ranges, and the often-extensive extent of MaR. Diastolic parameters in the acute setting and at 6-months follow up are presented in Table 6.

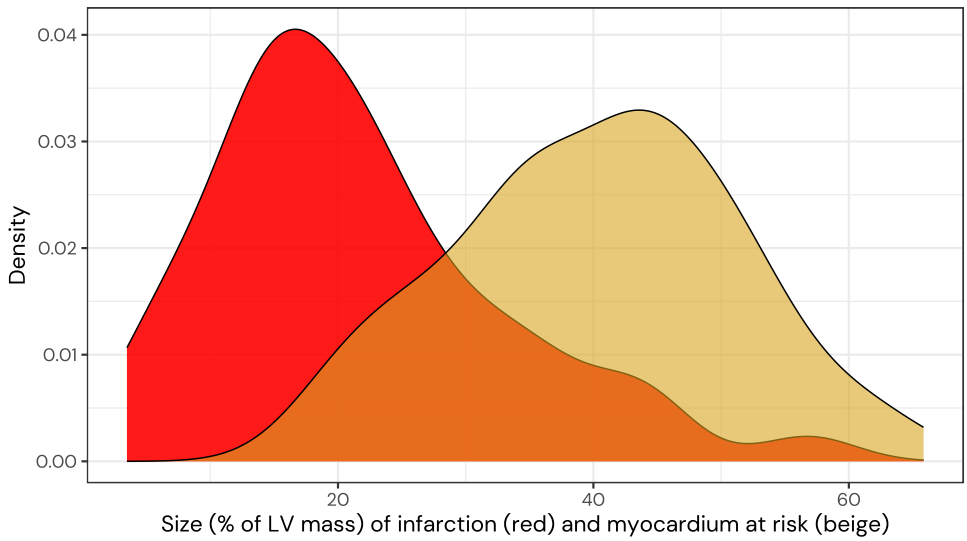

Figure 6. Distributions of IS and MaR. Density plots constructed from the actual distributions illustrating that MaR often is substantially larger than IS.

Diastolic dysfunction as defined by the guidelines[2] was present in 50% of patients at baseline and 21% at follow-up, although the distribution of the various parameters, both conventional and PDF, were within normal limits. Only 22% of patients had a tricuspid regurgitation where measurement of its Vmax was possible, and a decision was made to not analyze this parameter further.

The results of regression modeling of the associations between IS, MaR and the diastolic parameters in the acute setting are reported in Table 7 and the results from follow-up in Table 8. In the acute setting, IS had weak or moderate associations with LAVI, DT, and the stiffness parameter k (R^2 = 0.13, 0.24, and 0.21, respectively, $p < 0.05$ for all). The relationship between IS and the diastolic parameters is illustrated in Figure 7. Testing if MaR influenced the association between IS and the diastolic parameters, only in the case of e' did this result in a negligible increase in adjusted R^2 (8 percentage points, p = 0.02). At follow up, final IS had a range of 5–28% of LV mass and was associated with lower c (R^2 = 0.22, p = 0.001), and the derived parameters KFEI and tau (R^2 = 0.21 and 0.14, respectively, p = 0.002 and 0.02, respectively).

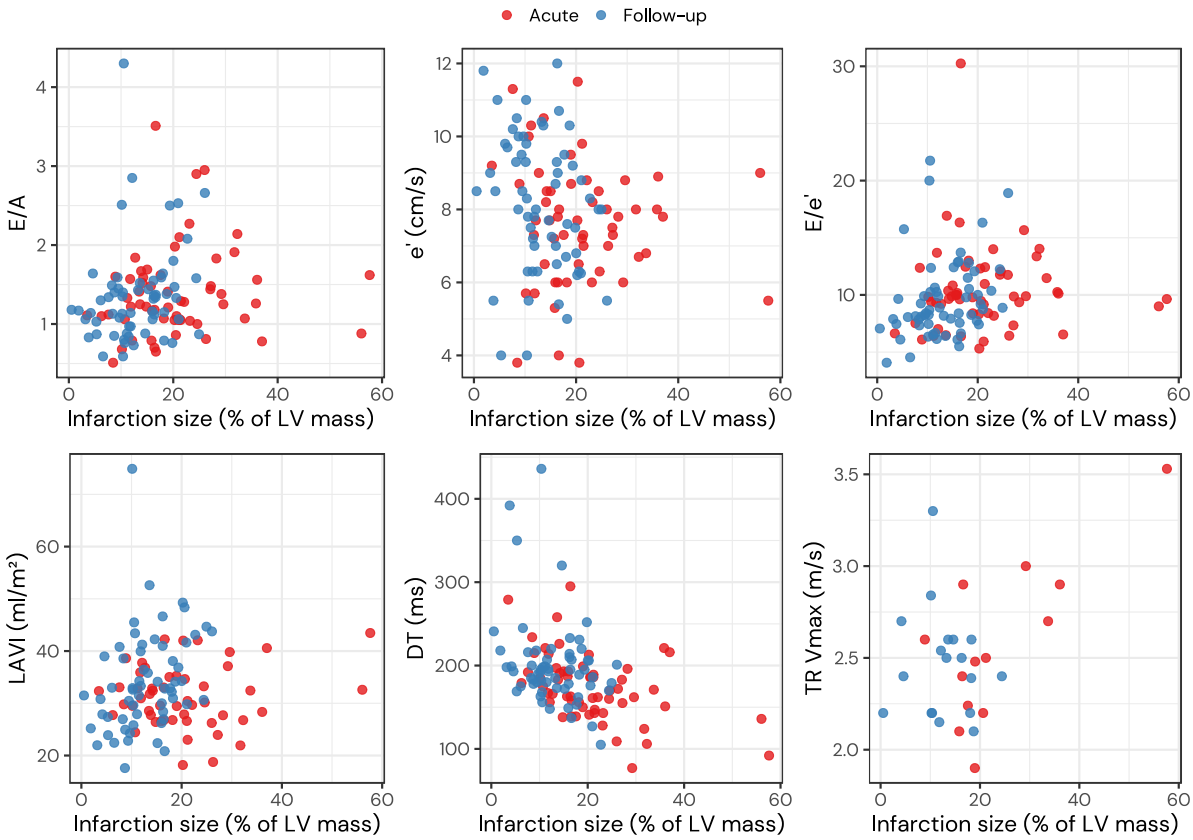

Figure 7a. Relationship between infarction size and conventional diastolic parameters acutely (red) and at 6 months follow-up (blue).

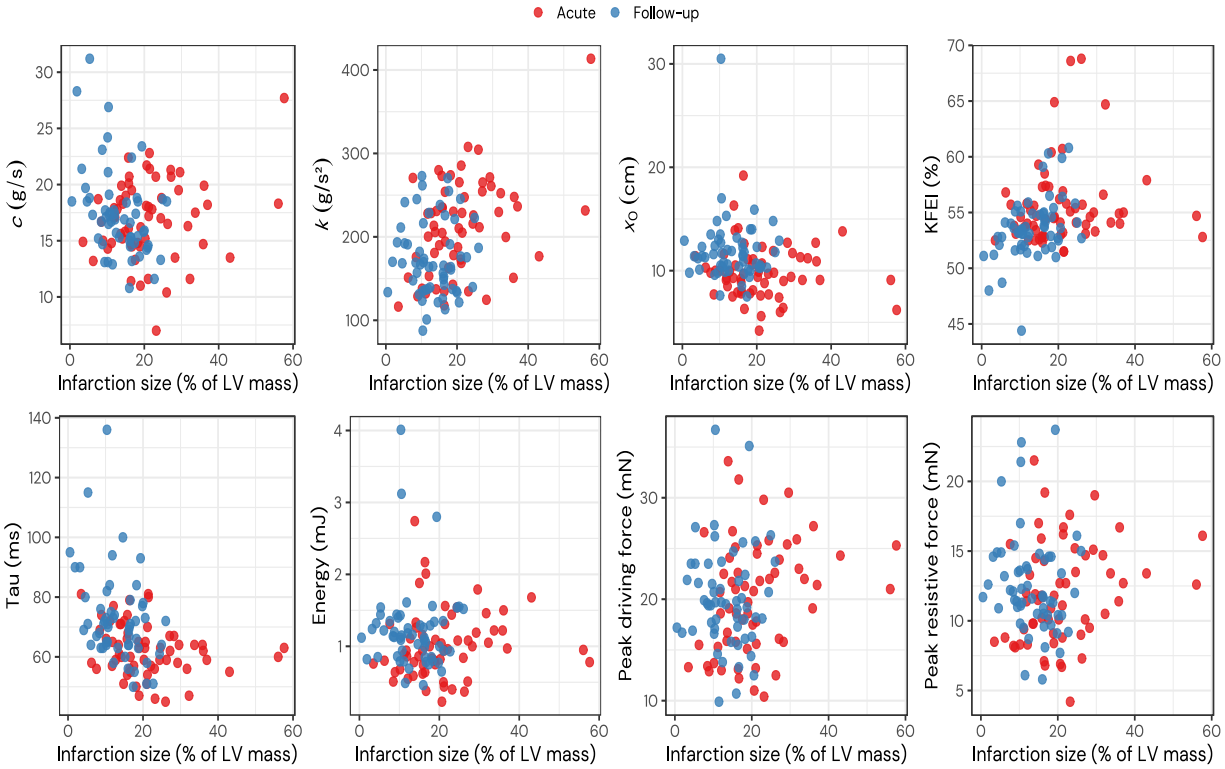

Figure 7b. Relationship between infarction size and PDF parameters acutely (red) and at 6 months follow-up (blue).

Table 5. Patient characteristics and CMR findings in Study III.

Number of subjects, n	74
Age, years	61 [55-68]
Male sex, n (%)	70 (95)
Hypertension, n (%)	24 (32)
Diabetes, n (%)	8 (11)
Infarction size, % of LV	17.9 [13.5–25.7]
Myocardium at risk, % of LV	42.0 [33.3–47.8]
LVEDV, ml	182 [160–219]
LV ejection fraction, %	50 [44–54]

Data presented as median [interquartile range], or number (n) and percent.
LV – left ventricular. LVEDV – left ventricular end-diastolic volume.

Table 6. Diastolic parameters from echocardiography at baseline and follow-up.

Parameter	Baseline	Follow-up
Number of subjects	74	61
E/A	1.26 [1.05–1.62]	1.30 [0.97–1.49]
e', cm/s	7.6 [6.2–8.5]	8.2 [6.8–9.6]
E/e'	9.9 [8.4–12.1]	8.5 [7.5–10.6]
DT, ms	169 [150–191]	193 [176–210]
LAVI, ml/m^2	31 [27–35]	33 [28–40]
TR Vmax, m/s	2.5 [2.2–2.9]	2.5 [2.2–2.6]
Diastolic dysfunction grading		
Normal, n (%)	26 (35)	36 (59)
Indeterminate, n (%)	11 (15)	12 (20)
Diastolic dysfunction, n (%)	37 (50)	13 (21)
Increased LAP, n (%)	8 (11)	3 (5)
PDF parameters		
c, g/s	17.2 [14.8–19.7]	16.9 [15.0–18.6]
k, g/s^2	213 [171–254]	166 [138–198]
x_0, cm	9.4 [8.0–11.1]	11.4 [10.3–12.8]
KFEI, %	54.6 [53.3–56.4]	53 [52–55]
Tau, ms	61 [57–67]	71 [64–77]
Filling energy, mJ	0.94 [0.68–1.26]	1.14 [0.86–1.35]
Peak DF, mN	20.2 [15.7–24.3]	19.6 [17.1–22.7]
Peak RF, mN	11.6 [9.0-14.7]	11.8 [10.5–14.5]

Data presented as median [IQR] or count (%). DT – deceleration time. LAVI – left atrial volume index. TR Vmax – tricuspid regurgitation maximum velocity. LAP – left atrial pressure. KFEI – kinematic filling efficiency index. DF – driving force. RF – resistive force.

Table 7. Regression model results in the acute setting

	IS as predictor			IS and MaR as predictors				Model comparison	
Parameter	IS effect	R^2	p*	IS effect	MaR effect	R^2	p*	Adj R^2 Δ	LR test p-value
E/A	0.08 [−0.12, 0.28]	0.01	0.73	0.04 [−0.28, 0.35]	0.09 [−0.25, 0.44]	0.01	0.92	−0.02	0.83
e′, cm/s	−0.5 [−1.1, 0.1]	0.04	0.28	0.4 [−0.5, 1.3]	−0.8 [−1.8, 0.2]	0.14	**0.04**	0.08	**0.02**
E/e′	0.5 [−0.9, 1.9]	0.01	0.72	−0.3 [−2.4, 1.7]	0.3 [−1.9, 2.5]	0.05	0.48	0.01	0.22
LAVI, ml/m²	−1 [−4, 1]	0.13	**0.01**	−2 [−6, 2]	3 [−1, 7]	0.17	**0.03**	<0.01	0.30
DT, ms	−26 [−38, −14]	0.24	**<0.001**	−27 [−46, −8]	7 [−14, 27]	0.25	**0.001**	−0.01	0.60
c, g/s	0.7 [−0.6, 2.0]	0.06	0.13	−1.0 [−3.0, 1.1]	2.3 [0.0, 4.5]	0.12	0.07	0.04	0.08
k, g/s²	35 [14, 55]	0.21	**<0.001**	25 [−7, 56]	20 [−15, 55]	0.22	**0.002**	−0.01	0.49
x_0, cm	−0.9 [−1.8, 0.04]	0.05	0.16	−0.8 [−2.2, 0.7]	−0.5 [−2.2, 1.1]	0.06	0.36	−0.02	0.68
KFEI, %	1.0 [−0.2, 2.3]	0.04	0.22	2.2 [0.2, 4.1]	−1.5 [−3.7, 0.6]	0.07	0.25	0.01	0.27
Tau, ms	−5 [−9, −1]	0.08	0.05	−10 [−16, −4]	5 [−1, 12]	0.13	**0.04**	0.03	0.11
Filling energy, mJ	0.00 [−0.18, 0.17]	<0.01	0.99	−0.06 [−0.33, 0.22]	0.01 [−0.30, 0.31]	0.01	0.94	−0.02	0.67
Peak DF, mN	1.6 [−0.5, 3.7]	0.05	0.16	1.1 [−2.2, 4.3]	0.2 [−3.4, 3.8]	0.06	0.40	−0.02	0.80
Peak RF, mN	0.7 [−0.7, 2.1]	0.03	0.32	−0.1 [−2.2, 2.0]	0.7 [−1.7, 3.0]	0.05	0.50	−0.01	0.55

Effect data reported as predicted differences in dependent parameters comparing the 1st and 3rd quartile of IS and MaR, with 95% confidence intervals. p* - p-value from model F-test. Adj R^2 Δ - difference in adjusted R^2. LR test p – p-value from likelihood ratio test. LAVI – left atrial volume index. DT – deceleration time. KFEI – kinematic filling efficiency index. DF – driving force. RF – resistive force.

Table 8. Regression model results at 6 months follow-up.

Parameter	Effect	R^2	p-value*
E/A	0.21 [−0.02, 0.43]	0.06	0.19
e′, cm/s	−0.6 [−1.3, 0.1]	0.06	0.19
E/e′	1.4 [0.2, 2.7]	0.09	0.08
LAVI, ml/m²	4 [0, 7]	0.10	0.05
DT, ms	−20 [−39, 0]	0.09	0.06
c, g/s	−2.0 [−3.3, −0.7]	0.22	**0.001**
k, g/s²	0.8 [−16.5, 18.1]	0.01	0.75
x_0, cm	−0.2 [−1.5, 1.0]	<0.01	0.89
KFEI, %	1.6 [0.7, 2.6]	0.21	**0.002**
Tau, ms	−7.1 [−12.6, −1.7]	0.14	**0.02**
Filling energy, mJ	−0.03 [−0.25, 0.20]	<0.01	0.97
Peak DF, mN	0.0 [−1.9, 2.0]	0.01	0.70
Peak RF, mN	−0.6 [−1.9, 0.7]	0.04	0.34

Effect data reported as predicted differences in dependent parameters comparing the 1st and 3rd quartile of final IS, with 95% confidence intervals. p* - p-value from model F-test. DT – deceleration time. LAVI – left atrial volume index. KFEI – kinematic filling efficiency index. DF – driving force. RF – resistive force.

5.4 Study IV

After excluding 5 patients with obvious cardiomyopathy (see 4.5.1), 123 patients with same day echocardiography and CMR examinations were available for analysis. According to the criteria for a normal echocardiogram, 33/123 (27%) were normal and 90/123 (73%) were pathological. Final diagnosis by CMR was TTS in 47 (38%), MI in 27 (22%), myocarditis in 23 (19%), and in 26 (21%) cases no definitive diagnosis could be established. Considering the patients with a normal echocardiogram, 3 (9%) had TTS, 10 (30%) had MI, 10 (30%) had myocarditis, and 10 (30%) had no diagnosis by CMR. Of the patients with a pathological echocardiogram, 16 (18%) had no diagnosis by CMR. The sensitivity, specificity, PPV, NPV, and likelihood ratios are presented in Table 9. The relationship between echocardiography results and final CMR diagnosis is illustrated in Figure 8.

The characteristics of patients with and without a diagnosis by CMR are presented in Table 10. Patients with a diagnosis by CMR had higher levels of hs-TnT and NT-pro-BNP, but with regards to imaging data, only the number of hypokinetic segments differed in a statistically significant manner.

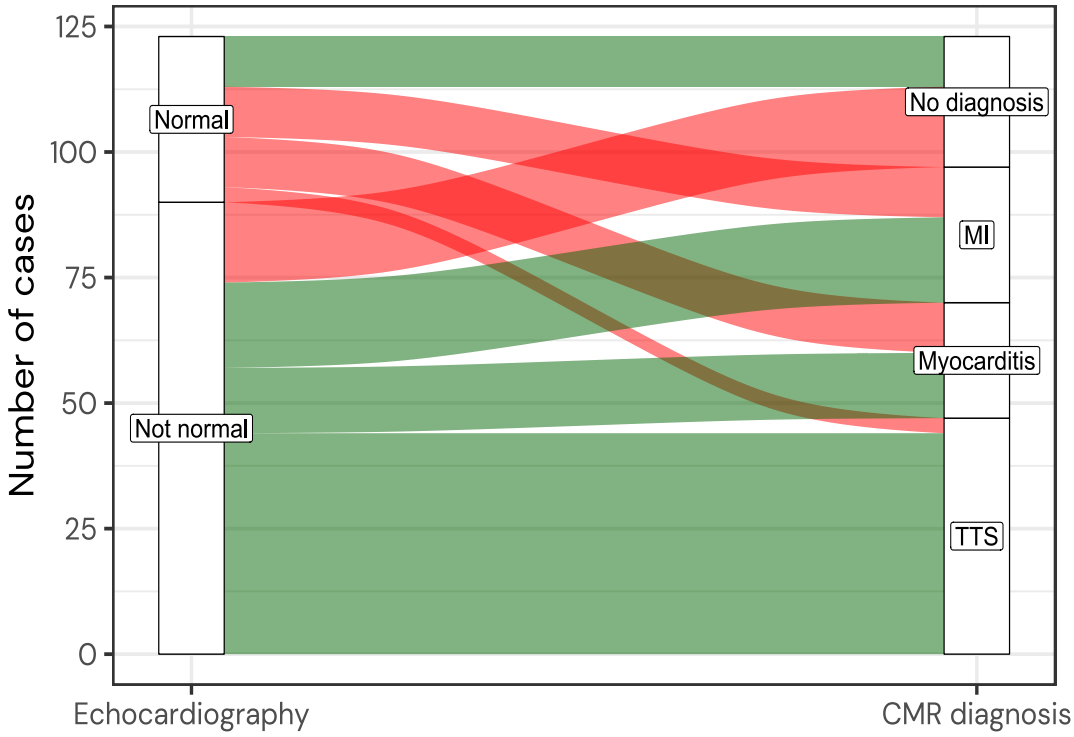

Figure 8. Echo assessment in relationship to CMR diagnosis. Alluvial plot showing final diagnosis by CMR in relationship to interpretation of the echocardiogram, with correct assessment in green and incorrect in red.

Table 9. Diagnostic performance of echocardiography compared to CMR.

Summary statistic	Value
Sensitivity	76%
Specificity	38%
Positive predictive value	82%
Negative predictive value	30%
Positive likelihood ratio	1.24
Inverse negative likelihood ratio	1.62

Table 10. Echocardiographic and laboratory findings, and demographic data.

	No CMR diagnosis (n = 26)	Any CMR diagnosis (n = 97)	p-value*	Missing (n)
Normal echocardiography, %	38	31	0.20	0
EF, %	57 [53–62]	57 [53–63]	0.76	9
GLS, %	17.6 [16.8–19.6]	17.7 [16.0–19.7]	0.54	17
Average e', cm/s	7.5 [6.5–8.6]	7.4 [6.1–9.1]	0.66	2
E/A ratio	1.01 [0.90–1.35]	1.03 [0.86–1.46]	0.93	0
E/e' ratio	8.9 [7.2–10.8]	8.7 [7.6–10.7]	0.77	1
LAVI, ml/m²	29 [24–33]	30 [27–35]	0.24	17
TR Vmax, m/s	2.2 [2.0–2.3]	2.2 [2.0–2.4]	0.26	42
Diastolic dysfunction, %	19	22	>0.99	24
RWMA present or not assessable, %	31	51	0.11	0
Hypokinetic segments, n	0 [0–1]	0 [0–3]	**0.03**	0
Troponin T, ng/L	21 [12–39]	116 [45–249]	**<0.001**	0
NT-pro-BNP, ng/L	128 [67–191]	282 [87–828]	**<0.001**	2
BNP/hs-TnT ratio	4.8 [3.5–7.2]	2.9 [0.5–11.5]	0.25	2
Age, years	59 [54–66]	61 [54–68]	0.32	0
Female sex, %	62	74	0.23	0

Data reported as percentages or median [interquartile range]. CMR – cardiac magnetic resonance imaging. EF – ejection fraction. GLS – global longitudinal strain. LAVI – left atrial volume index. TnT – troponin T. TR Vmax – tricuspid regurgitation maximal velocity. RWMA – regional wall motion abnormalities. *) p-value from the Wilcoxon rank sum test, or chi-square test for presence of diastolic dysfunction, RWMA and sex.

The distributions of CMR diagnoses per tertile of hs-TnT and NT-pro-BNP are illustrated in Figure 9. The probability of obtaining a CMR diagnosis was predicted from the logistic regression models and reported graphically in Figure 10, with model specifications in Table 11. The odds ratio for receiving a CMR diagnosis with a 10-unit increase in hs-TnT was 1.27 (95% CI 1.11–1.46), and 1.45 (95% CI 1.08–1.94) with a 100-unit increase in NT-pro-BNP, respectively. At normal levels of hs-TnT and NT-pro-BNP the predicted probability of a diagnosis by CMR was approximately 0.25 and 0.5, respectively. The predicted probability tended to be stronger with a pathological than normal echocardiogram for hs-TnT but did not differ for NT-pro-BNP.

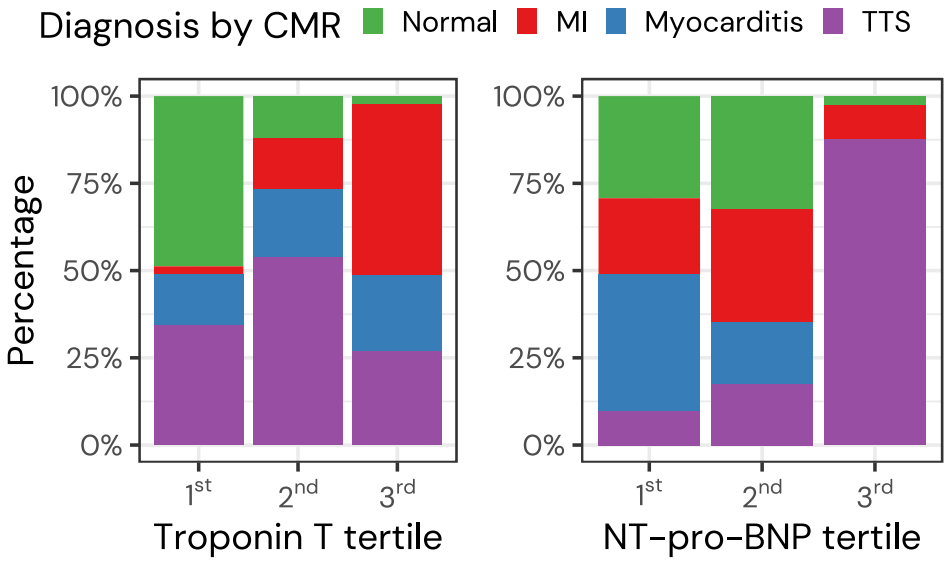

Figure 9. Distribution of CMR diagnoses by biomarker tertile group.

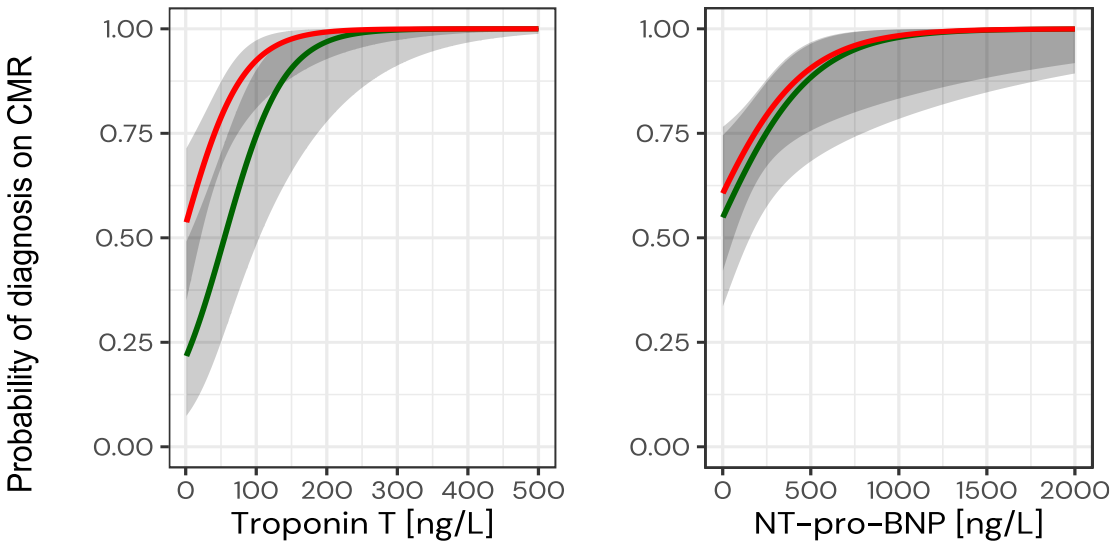

Figure 10. Predicted probability of CMR diagnosis using hs-TnT or NT-pro-BNP. Probability of receiving a diagnosis by CMR as a function of respective biomarker level. Green and red lines indicate predicted probabilities for normal and pathological echocardiograms, respectively, with shaded areas indicating 95% confidence intervals.

Table 11. Logistic regression model specifications.

hs-TnT model

Specification: CMR diagnosis (0/1) ~ hs-TnT + Pathological echo (0/1)

Number of observations: 123

Model likelihood ratio test χ^2 35.48, p<0.001

	Coefficient	Standard error	Wald Z	p
Intercept	-1.3058	0.6396	-2.04	0.041
hs-TnT	0.0238	0.0070	3.38	0.001
Pathological echo	1.4312	0.5995	2.39	0.017

NT-pro-BNP model

Specification: CMR diagnosis (0/1) ~ NT-pro-BNP + Pathological echo (0/1)

Number of observations: 121

Model likelihood ratio test χ^2 18.48, p<0.001

	Coefficient	Standard error	Wald Z	p
Intercept	0.1926	0.4488	0.43	0.668
NT-pro-BNP	0.0037	0.0015	2.48	0.013
Pathological echo	0.2362	0.4888	0.48	0.629

6 Discussion

6.1 A novel software application for PDF analysis

As a result of Study I, a new application for using the PDF method is now publicly available. To the best of our knowledge, there exists only one other available application[82], which however requires a paid programming platform and a cumbersome preparation of the DICOM images in multiple steps. By contrast, Echo E-waves is completely free and can read DICOM images directly from all major vendors of ultrasound equipment.

Using this interface, it was also shown that the PDF method has good intra- and interobserver variability, except for M and B. Of note, intraobserver variability was also tested in Study II, with similar results.

M and B are by definition the slope and intercept of a regression line between the products of $k \times x_0$ (peak driving force) and $c \times$ Vmax (peak resistive force). Even though there was a visually observed high degree of linearity and high R^2 values in all patients, reproducing earlier findings[46], the observer variability of the actual values of M and B was high. This is likely due to the nature of linear regression, where observations at the tails of the distribution can have a large effect on the slope of the regression line. This also entails that the decision to include or exclude a certain E-wave can have unpredictably high effects on the numerical results for M and B. A possible amelioration would be to induce a larger variation in load and acquire more E-waves during higher load. Notably, Shmuylovich *et al.* used a tilt board and achieved a range of peak driving force of 35-40 mN[46], while the post-Valsalva method used in this study resulted in a more modest 8 mN mean range. Due to these findings, we did not analyze M and B in Study III. Other loading methods, such as passive leg raise, should be explored.

6.1.1 Strengths and limitations

This is the first study describing and providing a freely available software application for PDF analysis. While the inter- and intraobserver variability assessed with different metrics in the study were good to excellent, the precision of the method in eventual clinical application is not known. We used multiple E-waves per patient, and the effect of using fewer remains to be evaluated. It also remains to be evaluated whether or not more advanced AI-supported Doppler analysis could improve accuracy and applicability.

6.2 Normal reference values for the PDF method

In Study II, a group of patients, who were likely to be healthy at least in terms of cardiovascular disease, was used to calculate normal reference values for the PDF method. The patients did not have a diagnosis of diabetes mellitus, hypertension, or atrial fibrillation, and had normal findings at resting and stress echocardiography. Together with Study I, this study can be used to facilitate the further application and interpretation of PDF analysis of diastolic function.

6.2.1 Strengths and limitations

Compared to other investigations into normal values for echocardiographic parameters, such as the NORRE Doppler substudy[83] with 449 subjects, this cohort is smaller. Furthermore, it does not consist of healthy volunteers. Rather, it consists of patients undergoing investigation for suspected disease. However, the patients selected for this study have been thoroughly screened, including for stress-induced myocardial ischemia, and therefore the prevalence of disease affecting diastolic function is likely to be minimal. We did not find any correlation with age, which seems unlikely, and this can probably be explained by a relative lack of older patients. In this study, we analyzed one E-wave per patient, and while this could reduce reproducibility of measurements on the individual level, it is unlikely to distort the distribution of the parameters for the whole group.

6.3 Diastolic function after myocardial infarction

The overall interpretation of the results of Study III is that the size of an acute myocardial infarction does not seem to be an important determinant of diastolic function, neither in the acute setting nor after 6 months. Furthermore, the myocardial edema of the MaR does not seem to have any meaningful impact on diastolic function. Weak associations were seen between IS and increased myocardial stiffness, shortened DT, and larger LAVI in the acute setting. After 6 months, patients with larger final IS had lower *c* representing less damping, and shorter tau and higher KFEI, the latter two being unsurprising as these parameters also reflect damping. There were no other statistically significant associations between final IS and the diastolic parameters.

While these findings might seem counterintuitive, they are in line with previous studies[67,69,72] also finding weak or no associations with IS. One study[67] showed a modest correlation between IS and increased peak E-wave velocity, which is in line with the present finding of increased stiffness. However, a correlation was also found with increased DT, as opposed to decreased DT in the present study. This latter discrepancy in findings is harder to reconcile. It is expected that the relationship between E-wave Vmax and DT (in the absence of mitral stenosis) is if anything inverse. In other words, the

higher Vmax is, the shorter DT would be. The earlier finding may be spurious or a reflection of confounding. Another study[69] found an association between IS and e', but not with E-wave Vmax or DT. The present study also reinforces previous findings that the myocardial edema of the MaR does not affect diastolic function in a clinically relevant way[70,72].

We also studied the relationship between diastolic measures and final IS at 6 months, and found statistical evidence for lower damping or viscoelastic energy loss with increasing IS. However, inspection of the data (Figure 7b) makes it plausible that this association is caused by influential outliers and does not represent a true pathophysiological relationship. Interestingly, there were no other statistically significant associations between final IS and the diastolic parameters, indicating that IS is not an important factor in diastolic dysfunction after a first MI. It should be noted that after 6 months it would not be unlikely that symptomatic heart failure would have led to treatments reducing filling pressures, in accordance with only 3 patients having echocardiographic findings supporting raised LAP. Other studies of diastolic function in the follow-up setting have examined patients between one[69] and up to three[67,70] months after MI. The implications of the differences in timing, and the likely interplay with LV remodeling remain to be investigated.

A general challenge in this field of inquiry is the difficulty of how to account for the loss of systolic function, and how this affects the parameters used to assess diastolic function that are dependent on systolic myocardial contraction. To what extent this is the explanation for the apparent dissociation of the extent of myocardial injury from diastolic function remains to be elucidated.

In summary, Study III suggests that after MI, signs of diastolic dysfunction should not be interpreted as indicating a large MI *per se*, prognostic implications of restrictive filling notwithstanding.

6.3.1 Strengths and limitations

The study sample is small, but nonetheless contains a wide range of IS which is a prerequisite for finding an association if one exists. Given the nature of this study, it was not possible to control for differences in loading conditions, which are well known to affect parameters of diastolic function. It is however not obvious that differences in loading conditions would have obscured the relationship between IS and diastolic function. We chose not to study the influence of medications, as we did not have detailed information regarding dosing or timing in relation to time of imaging. The intervention of the RECOND trial was not analyzed in the scope of the present study, as the primary outcome did not reach statistical significance, and also considering that it would introduce a multiplicity testing problem as we analyzed a large number of diastolic parameters. A further limitation is the apparent lack of diastolic dysfunction at

follow-up, at least considering the low prevalence of increased LAP. However, this is likely to be reflective of patient outcomes in contemporary practice, although it is noted that the sample was small. Finally, as this was a CMR-based study entailing the exclusion of patients with atrial fibrillation, and potentially also older patients with diabetes mellitus and hypertension due to concerns over contrast toxicity in impaired renal function, it is possible that patients "at risk" for developing diastolic dysfunction after MI were disproportionally excluded.

6.4 Utilization of echocardiography and CMR in MINOCA

It would be easy to assume that it is possible, using echocardiography and biomarkers, to identify a subset of MINOCA patients where CMR imaging may be futile. However, we found that a normal echocardiogram had low specificity and low negative predictive value for identifying patients receiving a diagnosis using early comprehensive CMR. Furthermore, the probability of a CMR diagnosis was substantial even at low or normal levels of hs-TnT and NT-pro-BNP. To the best of our knowledge, Study IV is the first to attempt to quantify the utility of echocardiography and biomarkers in this setting. Notably, among the patients with "false" normal echocardiograms almost a third had CMR evidence of MI. This is important since one could argue that the final diagnosis is moot if it does not entail a specific treatment strategy with clear prognostic implications. This could arguably be the case for myocarditis and TTS, but certainly not for MI.

We found an association between hs-TnT levels and probability of receiving a CMR diagnosis, both for patients with normal and pathological echocardiograms. This is in line with previous studies finding higher diagnostic yield in patients with hs-TnT above the cutoff maximizing sensitivity and specificity (Youden's J-index)[84], and a study where it was not possible to find a cutoff for hs-TnT that would give less than 15% false negatives[75]. Potentially at odds with this is one study where there were no pathological CMR findings in patients with hs-TnT < 100 ng/L and normal ECGs[85]. We did not include ECG findings in the present study. We also found an association between NT-pro-BNP levels and the probability of a CMR diagnosis, which does not seem to have been documented in the literature previously.

The findings of this study highlight the added value of myocardial tissue characterization by CMR, since myocardial edema and scarring can be visualized even when these pathological processes do not cause a readily detectable change in myocardial function. Also, levels of biomarkers, with which we have developed a familiarity with in the setting of type-1 MI and chronic heart failure, can be less helpful in new contexts.

6.4.1 Strength and limitations

In this study, the final diagnosis was the one resulting from CMR interpretation in the clinical setting of an ACS. While this should not affect the evaluation of to what extent patients with normal echocardiograms receive a CMR diagnosis, the nature of the false positives (pathological echocardiography but normal CMR) is not explained by the current study. As these patients also presented with signs and symptoms of an ACS leading to coronary angiography after clinical evaluation by a cardiologist, and had significantly elevated levels of hs-TnT, the lack of diagnostic CMR findings does not mean that these patients did not have an actual diagnosis. Also, the echocardiograms were read blinded for CMR diagnosis, but not for the fact that all patients were under investigation for MINOCA. This can have led to false positive assessments of RWMAs.

By study design, echocardiography and blood sampling was performed on the same day as the CMR examination. While this has the advantage of providing a snapshot of these different diagnostic methods at the same time, it is likely that, for example, even earlier echocardiography would be more sensitive for transient RWMAs. Considering the heterogeneity of underlying diagnoses, the optimal timing of blood sampling is also unknown.

We used levels of hs-TnT and NT-pro-BNP to derive predicted probabilities of obtaining a CMR diagnosis. While this has the advantage of providing a more clinically relevant indication of the interpretation of a certain biomarker elevation, we did not validate the underlying models further, and the results should be seen more as rough indicators of probability levels rather than exact predictions.

6.5 Echocardiography in MI – future perspectives

The value of echocardiography in MI is well established[86]. It stands as the go-to tool for clinicians needing a comprehensive and readily available evaluation of cardiac function after MI, with excellent capabilities to identify conditions of clinical importance such has heart failure and mechanical complications. However, as this thesis has illustrated, the associations between echocardiographic findings and underlying pathology are not always intuitive or straightforward. Of note, the development of diastolic dysfunction and heart failure after MI is of continued interest to investigate, as part of the broader goal of identifying patients for more tailored care and identification of patients at risk for adverse events. This requires future research using comprehensive baseline evaluation and sufficient follow-up. Likewise, the optimization of allocation of imaging resources deserves further attention, even though this ultimately could entail a recommendation for wider use of more advanced techniques such as CMR.

7 Conclusions

Overall, this thesis has evaluated echocardiographic methods in myocardial infarction patients using cardiovascular magnetic resonance imaging as a reference.

Specific conclusions are:

Study I: Analysis of diastolic function using the PDF method implemented in freely available semiautomatic software is highly feasible, time efficient, and has good to excellent intra-and interobserver variability.

Study II: Normal reference limits for PDF measures are provided, and can be useful for the interpretation of future clinical research.

Study III: The relationship between the spatial extent of myocardial injury after acute MI and the parameters used to assess diastolic function seems to be mediated by mechanisms beyond simply the spatial extent of ischemia or infarction.

Study IV: Echocardiography and biomarkers, while remaining generally useful in the work-up of suspected cardiac disease, should not be used to determine which patients with MINOCA should undergo a CMR examination, as such an approach will lead to many missed diagnoses.

8 Acknowledgements

When I was growing up, my parents **Marianne** and **Anders** used to say that I could pursue whatever career I wanted, as long as it involved using my brain. For this and many other things I am thankful for, as well as all the dinner discussions with you and my sister **Åsa** revolving around diseases and diagnoses; in the end my career in medicine was inevitable. I also wish to express my gratitude to several people who have supported and influenced me.

My main supervisor **Martin Ugander** for gently pushing me towards goals I did not know I was able to reach, and always having a fresh perspective and new ideas.

My co-supervisor **Per Tornvall**, also head of the Karolinska department at Södersjukhuset, for always being a steady hand, pointing towards solutions for every problem.

Patrik Norgren for being my true echocardiography mentor.

The echocardiography team at Hjärtlab for all the images, blurry and crisp, and all of the fun and general excellence: **Johan Wardell, Aleida Andrist, Maria Boberg & Ylva Fornander.**

Bengt Ullman for embodying the application of a scientific mindset in clinical practice.

Robin Hofmann for all discussions, past and future.

All the colleagues at the cardiology clinic at Södersjukhuset for providing companionship and a fun community in the flux of patients and politics, I'm looking forward to continuing working with you, with **Raffaele Scorza** at the helm.

Arne Olsson, unsurpassable in his succinctness in describing the art of echocardiography.

Mårten Rosenqvist for my first introduction into the world of clinical research.

Lis Kohlström, **Runa Sundelin** and **Gun Wedeen**, our trusted research nurses, for keeping everything in order and making things possible.

Although we haven't met - **Albert Støylen** for opening my eyes to many areas of echocardiography and physiology, **Frank Harrell** for changing my views on statistics, and the communities at **Stack Overflow** and **Cross Validated**, without which many things would have remained unsolved.

Last but not least my loving wife **Jessika** and the world's best two girls **Julia** and **Ines**, I love you above all else!

9 References

1. Nagueh SF, Appleton CP, Gillebert TC, Marino PN, Oh JK, Smiseth OA, Waggoner AD, Flachskampf FA, Pellikka PA, Evangelista A. Recommendations for the Evaluation of Left Ventricular Diastolic Function by Echocardiography. *J Am Soc Echocardiogr*. 2009;22:107–133.

2. Nagueh SF, Smiseth OA, Appleton CP, Byrd III BF, Dokainish H, Edvardsen T, Flachskampf FA, Gillebert TC, Klein AL, Lancellotti P, Marino P, Oh JK, Popescu BA, Waggoner AD. Recommendations for the Evaluation of Left Ventricular Diastolic Function by Echocardiography: An Update from the American Society of Echocardiography and the European Association of Cardiovascular Imaging. *J Am Soc Echocardiogr*. 2016;29:277–314.

3. Kim RJ, Fieno DS, Parrish TB, Harris K, Chen EL, Simonetti O, Bundy J, Finn JP, Klocke FJ, Judd RM. Relationship of MRI delayed contrast enhancement to irreversible injury, infarct age, and contractile function. *Circulation*. 1999;100:1992–2002.

4. Lønborg J, Vejlstrup N, Kelbæk H, Holmvang L, Jørgensen E, Helqvist S, Saunamäki K, Ahtarovski KA, Bøtker HE, Kim WY, Clemmensen P, Engstrøm T. Final infarct size measured by cardiovascular magnetic resonance in patients with ST elevation myocardial infarction predicts long-term clinical outcome: an observational study. *Eur Heart J Cardiovasc Imaging*. 2013;14:387–395.

5. Miller TD, Christian TF, Hopfenspirger MR, Hodge DO, Gersh BJ, Gibbons RJ. Infarct Size After Acute Myocardial Infarction Measured by Quantitative Tomographic 99mTc Sestamibi Imaging Predicts Subsequent Mortality. *Circulation*. 1995;92:334–341.

6. Burns RJ, Gibbons RJ, Yi Q, Roberts RS, Miller TD, Schaer GL, Anderson JL, Yusuf S. The relationships of left ventricular ejection fraction, end-systolic volume index and infarct size to six-month mortality after hospital discharge following myocardial infarction treated by thrombolysis. *J Am Coll Cardiol*. 2002;39:30–36.

7. Satoh H, Sano M, Suwa K, Saitoh T, Nobuhara M, Saotome M, Urushida T, Katoh H, Hayashi H. Distribution of late gadolinium enhancement in various types of cardiomyopathies: Significance in differential diagnosis, clinical features and prognosis. *World J Cardiol*. 2014;6:585–601.

8. Chamsi-Pasha MA, Zhan Y, Debs D, Shah DJ. CMR in the Evaluation of Diastolic Dysfunction and Phenotyping of HFpEF: Current Role and Future Perspectives. *JACC Cardiovasc Imaging*. 2020;13:283–296.

9. Ramos JG, Fyrdahl A, Wieslander B, Thalén S, Reiter G, Reiter U, Jin N, Maret E, Eriksson M, Caidahl K, Sörensson P, Sigfridsson A, Ugander M. Comprehensive Cardiovascular Magnetic Resonance Diastolic Dysfunction Grading Shows Very Good Agreement Compared With Echocardiography. *JACC Cardiovasc Imaging*. 2020;13:2530–2542.

10. Thygesen K, Alpert JS, Jaffe AS, Chaitman BR, Bax JJ, Morrow DA, White HD, Executive Group on behalf of the Joint European Society of Cardiology (ESC)/American College of Cardiology (ACC)/American Heart Association (AHA)/World Heart Federation (WHF) Task Force for the Universal Definition of Myocardial Infarction. Fourth Universal Definition of Myocardial Infarction (2018). *Circulation*. 2018;138:e618–e651.

11. Ibanez B, James S, Agewall S, Antunes MJ, Bucciarelli-Ducci C, Bueno H, Caforio ALP, Crea F, Goudevenos JA, Halvorsen S, Hindricks G, Kastrati A, Lenzen MJ, Prescott E, Roffi M, Valgimigli M, Varenhorst C, Vranckx P, Widimský P, ESC Scientific Document Group. 2017 ESC Guidelines for the management of acute myocardial infarction in patients presenting with ST-segment elevation: The Task Force for the management of acute myocardial infarction in patients presenting with ST-segment elevation of the European Society of Cardiology (ESC). *Eur Heart J*. 2018;39:119–177.

12. Croisille P, Kim HW, Kim RJ. Controversies in cardiovascular MR imaging: T2-weighted imaging should not be used to delineate the area at risk in ischemic myocardial injury. *Radiology*. 2012;265:12–22.

13. Jablonowski R, Engblom H, Kanski M, Nordlund D, Koul S, van der Pals J, Englund E, Heiberg E, Erlinge D, Carlsson M, Arheden H. Contrast-Enhanced CMR Overestimates Early Myocardial Infarct Size: Mechanistic Insights Using ECV Measurements on Day 1 and Day 7. *JACC Cardiovasc Imaging*. 2015;8:1379–1389.

14. Ibanez B, Aletras AH, Arai AE, Arheden H, Bax J, Berry C, Bucciarelli-Ducci C, Croisille P, Dall'Armellina E, Dharmakumar R, Eitel I, Fernández-Jiménez R, Friedrich MG, García-Dorado D, Hausenloy DJ, Kim RJ, Kozerke S, Kramer CM, Salerno M, Sánchez-González J, Sanz J, Fuster V. Cardiac MRI Endpoints in Myocardial Infarction Experimental and Clinical Trials: JACC Scientific Expert Panel. *J Am Coll Cardiol*. 2019;74:238–256.

15. Laine GA, Allen SJ. Left ventricular myocardial edema. Lymph flow, interstitial fibrosis, and cardiac function. *Circ Res*. 1991;68:1713–1721.

16. Weng ZC, Nicolosi AC, Detwiler PW, Hsu DT, Schierman SW, Goldstein AH, Spotnitz HM. Effects of crystalloid, blood, and University of Wisconsin perfusates on weight, water content, and left ventricular compliance in an edema-prone, isolated porcine heart model. *J Thorac Cardiovasc Surg*. 1992;103:504–513.

17. Miyamoto M, McClure DE, Schertel ER, Andrews PJ, Jones GA, Pratt JW, Ross P, Myerowitz PD. Effects of hypoproteinemia-induced myocardial edema on left ventricular function. *Am J Physiol*. 1998;274:H937-944.

18. Desai KV, Laine GA, Stewart RH, Cox CS Jr, Quick CM, Allen SJ, Fischer UM. Mechanics of the left ventricular myocardial interstitium: effects of acute and chronic myocardial edema. *Am J Physiol Heart Circ Physiol*. 2008;294:H2428-2434.

19. Dongaonkar RM, Stewart RH, Geissler HJ, Laine GA. Myocardial microvascular permeability, interstitial oedema, and compromised cardiac function. *Cardiovasc Res*. 2010;87:331–339.

20. Kidambi A, Mather AN, Swoboda P, Motwani M, Fairbairn TA, Greenwood JP, Plein S. Relationship between Myocardial Edema and Regional Myocardial Function after Reperfused Acute Myocardial Infarction: An MR Imaging Study. *Radiology*. 2013;267:701–708.

21. von Korn H, Graefe V, Ohlow M-A, Yu J, Huegl B, Wagner A, Gruene S, Lauer B. Acute Coronary Syndrome without Significant Stenosis on Angiography Characteristics and Prognosis. *Tex Heart Inst J*. 2008;35:406–412.

22. Pasupathy S, Air T, Dreyer RP, Tavella R, Beltrame JF. Systematic review of patients presenting with suspected myocardial infarction and nonobstructive coronary arteries. *Circulation*. 2015;131:861–870.

23. Lindahl B, Baron T, Erlinge D, Hadziosmanovic N, Nordenskjöld A, Gard A, Jernberg T. Medical Therapy for Secondary Prevention and Long-Term Outcome in Patients With Myocardial Infarction With Nonobstructive Coronary Artery Disease. *Circulation*. 2017;135:1481–1489.

24. Tamis-Holland JE, Jneid H, Reynolds HR, Agewall S, Brilakis ES, Brown TM, Lerman A, Cushman M, Kumbhani DJ, Arslanian-Engoren C, Bolger AF, Beltrame JF, American Heart Association Interventional Cardiovascular Care Committee of the Council on Clinical Cardiology; Council on Cardiovascular and Stroke Nursing; Council on Epidemiology and Prevention; and Council on Quality of Care and Outcomes Research. Contemporary Diagnosis and Management of Patients With Myocardial Infarction in the Absence of Obstructive Coronary Artery Disease: A Scientific Statement From the American Heart Association. *Circulation*. 2019;139:e891–e908.

25. Collste O, Sörensson P, Frick M, Agewall S, Daniel M, Henareh L, Ekenbäck C, Eurenius L, Guiron C, Jernberg T, Hofman-Bang C, Malmqvist K, Nagy E, Arheden H, Tornvall P. Myocardial infarction with normal coronary arteries is common and associated with normal findings on cardiovascular magnetic resonance imaging: results from the Stockholm Myocardial Infarction with Normal Coronaries study. *J Intern Med*. 2013;273:189–196.

26. Agewall S, Beltrame JF, Reynolds HR, Niessner A, Rosano G, Caforio ALP, De Caterina R, Zimarino M, Roffi M, Kjeldsen K, Atar D, Kaski JC, Sechtem U, Tornvall P, WG on Cardiovascular Pharmacotherapy. ESC working group position paper on myocardial infarction with non-obstructive coronary arteries. *Eur Heart J*. 2017;38:143–153.

27. Sörensson P, Ekenbäck C, Lundin M, Agewall S, Bacsovics Brolin E, Caidahl K, Cederlund K, Collste O, Daniel M, Jensen J, Y-Hassan S, Henareh L, Hofman-Bang C, Lyngå P, Maret E, Sarkar N, Spaak J, Winnberg O, Ugander M, Tornvall P. Early Comprehensive Cardiovascular Magnetic Resonance Imaging in Patients With Myocardial Infarction With Nonobstructive Coronary Arteries. *JACC Cardiovasc Imaging*. 2021;14:1774–1783.

28. Weiss JL, Frederiksen JW, Weisfeldt ML. Hemodynamic determinants of the time-course of fall in canine left ventricular pressure. *J Clin Invest*. 1976;58:751–760.

29. Kitabatake A, Inoue M, Asao M, Tanouchi J, Masuyama T, Abe H, Morita H, Senda S, Matsuo H. Transmitral blood flow reflecting diastolic behavior of the left ventricle in health and disease--a study by pulsed Doppler technique. *Jpn Circ J*. 1982;46:92–102.

30. Ohno M, Cheng CP, Little WC. Mechanism of altered patterns of left ventricular filling during the development of congestive heart failure. *Circulation*. 1994;89:2241–2250.

31. Appleton CP, Hatle LK, Popp RL. Relation of transmitral flow velocity patterns to left ventricular diastolic function: new insights from a combined hemodynamic and Doppler echocardiographic study. *J Am Coll Cardiol*. 1988;12:426–440.

32. Garcia MJ, Thomas JD, Klein AL. New Doppler echocardiographic applications for the study of diastolic function. *J Am Coll Cardiol*. 1998;32:865–875.

33. Nagueh SF, Sun H, Kopelen HA, Middleton KJ, Khoury DS. Hemodynamic determinants of the mitral annulus diastolic velocities by tissue Doppler. *J Am Coll Cardiol*. 2001;37:278–285.

34. Hasegawa H, Little WC, Ohno M, Brucks S, Morimoto A, Cheng H-J, Cheng C-P. Diastolic mitral annular velocity during the development of heart failure. *J Am Coll Cardiol*. 2003;41:1590–1597.

35. Nagueh SF, Middleton KJ, Kopelen HA, Zoghbi WA, Quiñones MA. Doppler tissue imaging: a noninvasive technique for evaluation of left ventricular relaxation and estimation of filling pressures. *J Am Coll Cardiol*. 1997;30:1527–1533.

36. Ommen SR, Nishimura RA, Appleton CP, Miller FA, Oh JK, Redfield MM, Tajik AJ. Clinical utility of Doppler echocardiography and tissue Doppler imaging in the estimation of left ventricular filling pressures: A comparative simultaneous Doppler-catheterization study. *Circulation*. 2000;102:1788–1794.

37. Nagueh SF, Abraham TP, Aurigemma GP, Bax JJ, Beladan C, Browning A, Chamsi-Pasha MA, Delgado V, Derumeaux G, Dolci G, Donal E, Edvardsen T, El Tallawi KC, Ernande L, Esposito R, Flachskampf FA, Galderisi M, Gentry J, Goldstein SA, Harb SC, Hubert A, Hung J, Klein AL, Lancellotti P, Mahmood RZ, Marino P, Popescu BA, Previato M, Sanghai SR, Smiseth OA, Xu J, for Diastolic Function Assessment Collaborators. Interobserver Variability in Applying American Society of Echocardiography/European Association of Cardiovascular Imaging 2016 Guidelines for Estimation of Left Ventricular Filling Pressure. *Circ Cardiovasc Imaging*. 2019;12:e008122.

38. Almeida JG, Fontes-Carvalho R, Sampaio F, Ribeiro J, Bettencourt P, Flachskampf FA, Leite-Moreira A, Azevedo A. Impact of the 2016 ASE/EACVI recommendations on the prevalence of diastolic dysfunction in the general population. *Eur Heart J Cardiovasc Imaging*. 2018;19:380–386.

39. Brutsaert DL, Rademakers FE, Sys SU. Triple control of relaxation: implications in cardiac disease. *Circulation*. 1984;69:190–196.

40. Ha J-W, Andersen OS, Smiseth OA. Diastolic Stress Test: Invasive and Noninvasive Testing. *JACC Cardiovasc Imaging*. 2020;13:272–282.

41. Altman DG, Royston P. The cost of dichotomising continuous variables. *BMJ*. 2006;332:1080.

42. Kovács SJ Jr, Barzilai B, Pérez JE. Evaluation of diastolic function with Doppler echocardiography: the PDF formalism. *Am J Physiol*. 1987;252:H178-187.

43. Lisauskas JB, Singh J, Bowman AW, Kovács SJ. Chamber properties from transmitral flow: prediction of average and passive left ventricular diastolic stiffness. *J Appl Physiol*. 2001;91:154–162.

44. Zhang W, Chung CS, Riordan MM, Wu Y, Shmuylovich L, Kovacs SJ. The Kinematic Filling Efficiency Index of the Left Ventricle: Contrasting Normal vs. Diabetic Physiology. *Ultrasound Med Biol*. 2007;33:842–850.

45. Mossahebi S, Kovács SJ. Kinematic Modeling Based Decomposition of Transmitral Flow (Doppler E-Wave) Deceleration Time into Stiffness and Relaxation Components. *Cardiovasc Eng Technol*. 2014;5:25–34.

46. Shmuylovich L, Kovács SJ. Load-independent index of diastolic filling: model-based derivation with in vivo validation in control and diastolic dysfunction subjects. *J Appl Physiol*. 2006;101:92–101.

47. Hall AF, Kovács SJ. Automated method for characterization of diastolic transmitral doppler velocity contours: Early rapid filling. *Ultrasound Med Biol*. 1994;20:107–116.

48. Kovács SJ, Rosado J, Manson McGuire AL, Hall AF. Can transmitral Doppler E-waves differentiate hypertensive hearts from normal? *Hypertension*. 1997;30:788–795.

49. Rich MW, Stitziel NO, Kovács SJ. Prognostic value of diastolic filling parameters derived using a novel image processing technique in patients > or = 70 years of age with congestive heart failure. *Am J Cardiol*. 1999;84:82–86.

50. Riordan MM, Chung CS, Kovács SJ. Diabetes and diastolic function: stiffness and relaxation from transmitral flow. *Ultrasound Med Biol*. 2005;31:1589–1596.

51. Caporizzo MA, Prosser BL. Need for Speed: The Importance of Physiological Strain Rates in Determining Myocardial Stiffness. *Front Physiol* [Internet]. 2021 [cited 2022 Dec 14];12. Available from: https://www.frontiersin.org/articles/10.3389/fphys.2021.696694

52. Isaaz K, Munoz del Romeral L, Lee E, Schiller NB. Quantitation of the motion of the cardiac base in normal subjects by Doppler echocardiography. *J Am Soc Echocardiogr Off Publ Am Soc Echocardiogr*. 1993;6:166–176.

53. Riordan MM, Kovács SJ. Quantitation of mitral annular oscillations and longitudinal "ringing" of the left ventricle: a new window into longitudinal diastolic function. *J Appl Physiol Bethesda Md 1985*. 2006;100:112–119.

54. Keren G, Meisner JS, Sherez J, Yellin EL, Laniado S. Interrelationship of mid-diastolic mitral valve motion, pulmonary venous flow, and transmitral flow. *Circulation*. 1986;74:36–44.

55. Ghosh E, Caruthers SD, Kovács SJ. E-wave generated intraventricular diastolic vortex to L-wave relation: model-based prediction with in vivo validation. *J Appl Physiol Bethesda Md 1985*. 2014;117:316–324.

56. Diamond G, Forrester JS. Effect of Coronary Artery Disease and Acute Myocardial Infarction on Left Ventricular Compliance in Man. *Circulation*. 1972;45:11–19.

57. Limbourg P, Just H, Lang KF. Left ventricular function after acute myocardial infarction. *Eur J Intensive Care Med*. 1976;2:7–11.

58. Forrester JS, Diamond G, Parmley WW, Swan HJ. Early increase in left ventricular compliance after myocardial infarction. *J Clin Invest*. 1972;51:598–603.

59. Bertrand ME, Lablanche JM, Fourrier JL, Traisnel G, Mirsky I. Left ventricular systolic and diastolic function during acute coronary artery balloon occlusion in humans. *J Am Coll Cardiol*. 1988;12:341–347.

60. Stewart JT, Grbic M, Sigwart U. Left atrial and left ventricular diastolic function during acute myocardial ischaemia. *Br Heart J*. 1992;68:377–381.

61. Labovitz AJ, Lewen MK, Kern M, Vandormael M, Deligonal U, Kennedy HL. Evaluation of left ventricular systolic and diastolic dysfunction during transient myocardial ischemia produced by angioplasty. *J Am Coll Cardiol*. 1987;10:748–755.

62. Bowman LK, Cleman MW, Cabin HS, Zaret BL, Jaffe CC. Dynamics of early and late left ventricular filling determined by Doppler two-dimensional echocardiography during percutaneous transluminal coronary angioplasty. *Am J Cardiol*. 1988;61:541–545.

63. Werner GS, Sold G, Teichmann D, Andreas S, Kreuzer H, Wiegand V. Impaired relationship between Doppler echocardiographic parameters of diastolic function and left ventricular filling pressure during acute ischemia. *Am Heart J*. 1990;120:63–72.

64. Whalley GA, Gamble GD, Doughty RN. Restrictive diastolic filling predicts death after acute myocardial infarction: systematic review and meta-analysis of prospective studies. *Heart Br Card Soc*. 2006;92:1588–1594.

65. Prasad SB, Lin AK, Guppy-Coles KB, Stanton T, Krishnasamy R, Whalley GA, Thomas L, Atherton JJ. Diastolic Dysfunction Assessed Using Contemporary Guidelines and Prognosis Following Myocardial Infarction. *J Am Soc Echocardiogr Off Publ Am Soc Echocardiogr*. 2018;31:1127–1136.

66. Byrne RA, Ndrepepa G, Braun S, Tiroch K, Mehilli J, Schulz S, Schömig A, Kastrati A. Peak Cardiac Troponin-T Level, Scintigraphic Myocardial Infarct Size and One-Year Prognosis in Patients Undergoing Primary Percutaneous Coronary Intervention for Acute Myocardial Infarction. *Am J Cardiol*. 2010;106:1212–1217.

67. Johannessen KA, Cerqueira MD, Stratton JR. Influence of myocardial infarction size on radionuclide and Doppler echocardiographic measurements of diastolic function. *Am J Cardiol*. 1990;65:692–697.

68. Yong Y, Nagueh SF, Shimoni S, Shan K, He ZX, Reardon MJ, Letsou GV, Howell JF, Verani MS, Quiñones MA, Zoghbi WA. Deceleration time in ischemic cardiomyopathy: relation to echocardiographic and scintigraphic indices of myocardial viability and functional recovery after revascularization. *Circulation*. 2001;103:1232–1237.

69. Barbieri A, Bursi F, Politi L, Rossi L, Fiocchi F, Ligabue G, Pingitore A, Positano V, Torricelli P, Modena MG. Echocardiographic diastolic dysfunction and magnetic resonance infarct size in healed myocardial infarction treated with primary angioplasty. *Echocardiography*. 2008;25:575–583.

70. Søholm H, Lønborg J, Andersen MJ, Vejlstrup N, Engstrøm T, Hassager C, Møller JE. Association diastolic function by echo and infarct size by magnetic resonance imaging after STEMI. *Scand Cardiovasc J SCJ*. 2016;50:172–179.

71. Azarisman SM, Carbone A, Shirazi M, Bradley J, Teo KS, Worthley MI, Worthley SG. Characterisation of Myocardial Injury via T1 Mapping in Early Reperfused Myocardial Infarction and its Relationship with Global and Regional Diastolic Dysfunction. *Heart Lung Circ*. 2016;25:1094–1106.

72. Chung H, Yoon J-H, Yoon YW, Park CH, Ko EJ, Kim JY, Min P-K, Kim TH, Lee BK, Hong B-K, Rim S-J, Kwon HM, Choi E-Y. Different contribution of extent of myocardial injury to left ventricular systolic and diastolic function in early reperfused acute myocardial infarction. *Cardiovasc Ultrasound*. 2014;12:6.

73. Gerbaud E, Arabucki F, Nivet H, Barbey C, Cetran L, Chassaing S, Seguy B, Lesimple A, Cochet H, Montaudon M, Laurent F, Bar O, Tearney GJ, Coste P. OCT and CMR for the Diagnosis of Patients Presenting With MINOCA and Suspected Epicardial Causes. *JACC Cardiovasc Imaging*. 2020;13:2619–2631.

74. Occhipinti G, Bucciarelli-Ducci C, Capodanno D. Diagnostic pathways in myocardial infarction with non-obstructive coronary artery disease (MINOCA). *Eur Heart J Acute Cardiovasc Care*. 2021;10:813–822.

75. Reynolds HR, Maehara A, Kwong RY, Sedlak T, Saw J, Smilowitz NR, Mahmud E, Wei J, Marzo K, Matsumura M, Seno A, Hausvater A, Giesler C, Jhalani N, Toma C, Har B, Thomas D, Mehta LS, Trost J, Mehta PK, Ahmed B, Bainey KR, Xia Y, Shah B, Attubato M, Bangalore S, Razzouk L, Ali ZA, Merz NB, Park K, Hada E, Zhong H, Hochman JS. Coronary Optical Coherence Tomography and Cardiac Magnetic Resonance Imaging to Determine Underlying Causes of Myocardial Infarction With Nonobstructive Coronary Arteries in Women. *Circulation*. 2021;143:624–640.

76. Verouhis D, Sörensson P, Gourine A, Henareh L, Persson J, Saleh N, Settergren M, Sundqvist M, Tornvall P, Witt N, Böhm F, Pernow J. Effect of remote ischemic conditioning on infarct size in patients with anterior ST-elevation myocardial infarction. *Am Heart J*. 2016;181:66–73.

77. Quiñones MA, Otto CM, Stoddard M, Waggoner A, Zoghbi WA. Recommendations for quantification of Doppler echocardiography: A report from the Doppler quantification task force of the nomenclature and standards committee of the American Society of Echocardiography. *J Am Soc Echocardiogr*. 2002;15:167–184.

78. Shmuylovich L. Kinematic Modeling of the Determinants of Diastolic Function [Internet]. Arts & Sciences Electronic Theses and Dissertations; 2015. Available from: http://openscholarship.wustl.edu/art_sci_etds/445

79. Lang RM, Badano LP, Mor-Avi V, Afilalo J, Armstrong A, Ernande L, Flachskampf FA, Foster E, Goldstein SA, Kuznetsova T, Lancellotti P, Muraru D, Picard MH, Rietzschel ER, Rudski L, Spencer KT, Tsang W, Voigt J-U. Recommendations for cardiac chamber quantification by echocardiography in adults: an update from the American Society of Echocardiography and the European Association of Cardiovascular Imaging. *J Am Soc Echocardiogr*. 2015;28:1-39.e14.

80. Harrell F. Regression Modeling Strategies: With Applications to Linear Models, Logistic and Ordinal Regression, and Survival Analysis [Internet]. 2nd ed. Springer International Publishing; 2015 [cited 2019 May 3]. Available from: https://www.springer.com/gp/book/9783319194240

81. R Core Team. R: A Language and Environment for Statistical Computing [Internet]. Vienna, Austria: R Foundation for Statistical Computing; 2021. Available from: https://www.R-project.org/

82. Mossahebi S, Zhu S, Chen H, Shmuylovich L, Ghosh E, Kovács SJ. Quantification of global diastolic function by kinematic modeling-based analysis of transmitral flow via the parametrized diastolic filling formalism. *J Vis Exp JoVE*. 2014;e51471.

83. Caballero L, Kou S, Dulgheru R, Gonjilashvili N, Athanassopoulos GD, Barone D, Baroni M, Cardim N, Gomez de Diego JJ, Oliva MJ, Hagendorff A, Hristova K, Lopez T, Magne J, Martinez C, de la Morena G, Popescu BA, Penicka M, Ozyigit T, Rodrigo Carbonero JD, Salustri A, Van De Veire N, Von Bardeleben RS, Vinereanu D, Voigt J-U, Zamorano JL, Bernard A, Donal E, Lang RM, Badano LP, Lancellotti P. Echocardiographic reference ranges for normal cardiac Doppler data: results from the NORRE Study. *Eur Heart J Cardiovasc Imaging*. 2015;16:1031–1041.

84. Williams MGL, Liang K, De Garate E, Spagnoli L, Fiori E, Dastidar A, Benedetto U, Biglino G, Johnson TW, Luscher T, Bucciarelli-Ducci C. Peak Troponin and CMR to Guide Management in Suspected ACS and Nonobstructive Coronary Arteries. *JACC Cardiovasc Imaging*. 2022;15:1578–1587.

85. Pathik B, Raman B, Mohd Amin NH, Mahadavan D, Rajendran S, McGavigan AD, Grover S, Smith E, Mazhar J, Bridgman C, Ganesan AN, Selvanayagam JB. Troponin-positive chest pain with unobstructed coronary arteries: incremental diagnostic value of cardiovascular magnetic resonance imaging. *Eur Heart J Cardiovasc Imaging*. 2016;17:1146–1152.

86. Feigenbaum H. Role of echocardiography in acute myocardial infarction. *Am J Cardiol*. 1990;66:17H-22H.